ChemComm

ROYAL SOCIETY OF CHEMISTRY

FEATURE ARTICLE

View Article Online
View Journal | View Issue

Cite this: *Chem. Commun.*, 2026, **62**, 8791

Therapeutic embolic agents for targeted drug delivery in transcatheter therapies: a review

Keren Zhao,[a] Peng Chen,[a] George Varghese P. J.,[a] Mohammad-Reza Hosseini-Siyanaki,[b] Reza Talaie,[b] Amirhossein Arzani,[cd] Charles Kim[e] and Jingjie Hu *[a]

Embolization has evolved from a purely mechanical occlusion technique to a multifunctional platform that supports imaging enhancement and therapeutic functions, including localized drug delivery, immunotherapy, and vascular remodeling. Although reviews on embolic agents have been published, the therapeutic performance of embolic platforms has not yet been systematically examined from a materials perspective linking material design and formation mechanisms to drug loading, release behavior, and therapeutic outcomes. In this review, we discuss the embolic system design principles and mechanisms underlying both clinically used and emerging embolic agents, emphasizing liquid/gel systems and microsphere (MS)-based platforms with integrated therapeutic functionality. We highlight how material design governs catheter delivery, vascular penetration, occlusion stability, and controlled drug release, key factors that govern the performance of all embolic categories. For liquid/gel embolics, we summarize clinical formulations alongside their reported outcomes, and we review emerging systems according to their mechanisms of solidification and biological interaction, including thermo-responsive gels, chemically triggered networks, complex coacervates, and shear-thinning nanocomposites. For MS embolics, we summarize clinically used materials and discuss emerging systems, focusing on how polymer chemistry, cross-linking, and network architecture regulate drug loading and release. Finally, we discuss key translational challenges in the emerging embolic systems and highlight opportunities for future embolic platforms that enable more precise and durable therapeutic control.

Received 17th February 2026,
Accepted 13th April 2026

DOI: 10.1039/d6cc01050d

rsc.li/chemcomm

1. Introduction

Transcatheter therapies represent a cornerstone of modern interventional medicine, enabling minimally invasive treatment for localized tumors, vascular malformations, and benign conditions. Compared with traditional open surgery, these procedures enable localized treatment with benefits including reduced pain, shorter hospital stays, and fewer complications.[2,3] By selectively occluding blood vessels, embolization deprives oxygen and nutrients from target tissues, leading to tumor necrosis, hemostasis, or attenuation of abnormal vascular activity. It provides a safe and effective alternative for patients who are not candidates for conventional open surgery.

In recent years, research has expanded beyond mechanical vessel occlusion toward therapeutic embolization. In this approach, embolic agents are also designed to deliver active therapeutic substances such as chemotherapeutic drugs, radioactive isotopes, anti-inflammatory agents, or biologics.[1] In oncology, transarterial chemoembolization (TACE)[2] and transarterial radioembolization (TARE)[3,4] have become standard-of-care treatments for unresectable liver cancer, providing localized delivery of chemotherapy or radiation. In vascular and neurointerventional radiology, embolization is used to manage aneurysms,[5] arteriovenous malformations (AVMs),[6] and internal hemorrhage.[7] Additionally, embolization has proven effective in managing benign and non-oncologic conditions including uterine fibroids[8] and benign prostatic hyperplasia,[9] underscoring the broad therapeutic utility of embolization. Across these applications, drug-loaded embolic agents enable localized and sustained release at the target site, thereby enhances therapeutic efficacy while minimizing systemic exposure and toxicity[10] (Fig. 1).

[a] *Department of Mechanical and Aerospace Engineering, North Carolina State University, Raleigh, NC, 27606, USA. E-mail: jingjiehu@ncsu.edu*
[b] *Division of Interventional Radiology, Department of Radiology, University of Minnesota, Minneapolis, MN, 55455, USA*
[c] *Department of Mechanical Engineering, University of Utah, Salt Lake City, UT, USA*
[d] *Scientific Computing and Imaging Institute, University of Utah, Salt Lake City, UT, USA*
[e] *Division of Vascular and Interventional Radiology, Department of Radiology, Duke University Medical Center, Durham, NC, USA*

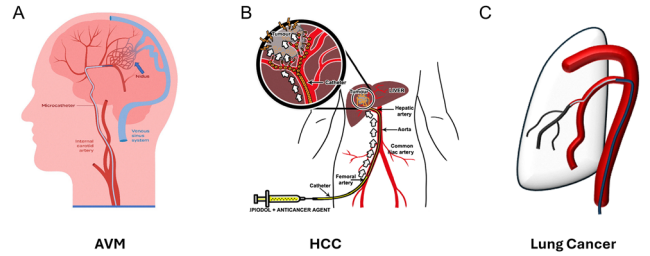

Fig. 1 Representative clinical conditions for therapeutic embolization, such as (A). Arteriovenous malformation (AVM). Reproduced from ref. 11, under the terms of the CC BY 4.0 license. (B) Hepatocellular carcinoma (HCC) showing tumor-feeding arterial supply targeted during embolization. (B) is reproduced with permission from ref. 12. Copyright 2013, Elsevier. (C). Lung cancer highlighting abnormal tumor-associated vasculature accessible by endovascular intervention.

The performance of embolic agents is fundamentally governed by both material design and the efficacy of the incorporated therapeutic components. From a performance perspective, embolic agents must enable smooth catheter delivery, effective vascular penetration, and stable vessel occlusion under physiological conditions. Once deployed, local hemodynamic forces govern embolic transport, spatial distribution, and retention within the vasculature.[13] In parallel, therapeutic efficacy requires sufficient therapeutic-loading capacity, predictable release kinetics, and stability within the biological environment. Achieving these objectives demands careful optimization of multiple interdependent material properties to balance mechanical reliability, deliverability, and therapeutic functionality.

At the material level, these performance requirements arise from key properties, such as rheological behavior, and other

Keren Zhao

Keren Zhao is a PhD candidate in Mechanical and Aerospace Engineering at North Carolina State University, holding master's degrees in Engineering Mechanics, and Industrial Engineering. Her research lies at the intersection of mechanics, soft matter, and biological validation. She studies soft material with tunable microstructure that reorganizes under mechanical fields to optimize macroscopic performance. Her current work focuses on injectable soft material for minimally invasive applications, with an emphasis on understanding how material properties influence stability and performance in physiological environments and translating these insights into clinically relevant solutions.

Peng Chen

Peng Chen received his master's degrees in chemical engineering and materials engineering from the University of Dayton, United States, in 2019 and 2022. He recently defended his PhD in mechanical engineering at North Carolina State University under the supervision of Prof. Jingjie Hu and is graduating in May 2026. His research focuses on the mechanical and physical behavior of embolic microspheres. His work integrates experimental characterization techniques such as rheology, AFM, and microfluidic-based testing to understand structure–property relationships and optimize microsphere performance for embolization therapies.

George Varghese P. J.

George Varghese P. J. is a PhD graduate in Mechanical Engineering from the Hu Research Group at North Carolina State University. He holds a master's degree in Materials Science and Engineering and a bachelor's degree in Polymer Science and Engineering. His work lies at the intersection of materials science, biomechanics, and biomedical applications. His doctoral research focused on the development of catheter-injectable hydrogels for minimally invasive embolization procedures. His broader research interests include polymers, biomaterials, nanotechnology, and the mechanical properties of materials.

Jingjie Hu

Jingjie Hu is an Assistant Professor in the Department of Mechanical and Aerospace Engineering at North Carolina State University and an Associate Faculty member in the Lampe Joint Department of Biomedical Engineering at NC State and UNC Chapel Hill. She received her PhD in Mechanical Engineering from Princeton University in 2018 and completed postdoctoral training at Mayo Clinic before joining NC State in 2021. Her research lies at the interface of mechanics, materials science, and bioengineering, with a focus on translational biomaterials, vascular devices, adhesion and cell mechanics.

physicochemical properties. These characteristics govern how embolic agents retain therapeutic payloads, respond to flow conditions, maintain structural integrity after delivery, and ultimately determine clinically relevant outcomes such as injectability, vascular stability, and drug release kinetics.

Physical properties, such as material form (*e.g.* liquid/gel, solid), influence catheter-based deliverability, vascular penetration, and distribution throughout target vessels.[14,15] Mechanical properties, including viscosity and elasticity, affect the ease of delivery through microcatheters and its ability to conform to vessel morphology without causing injury. Mechanical stability under physiological conditions is essential to prevent adverse effects such as fragmentation, migration, or recanalization.[16] Imageability enables real-time monitoring during delivery and facilitates post-procedural assessment.[17] It is typically achieved by incorporating contrast agents that are compatible with imaging modalities such as fluoroscopy, ultrasound, and near-infrared fluorescence (NIR).[18] Biocompatibility and hemocompatibility ensure that embolic agents do not trigger adverse immune reactions, inflammation, or toxicity upon interaction with biological tissues.

Finally, drug-loading capability allows embolic agents to carry and control the release of therapeutic agents such as chemotherapeutic drugs, radioactive isotopes, or bioactive molecules.[18,19] This enables localized and sustained treatment at the target site. It affects therapeutic efficacy while minimizing off-target effects and systemic toxicity compared to conventional systemic drug administration. Together, these considerations highlight the central role of material design of therapeutic embolic agents.

The development of embolic systems for therapeutic applications is ongoing, with significant advances in material design and delivery physics. However, clinical evidence remains limited and requires further accumulation. Conventional transarterial chemoembolization (cTACE) using liquid agents such as lipiodol, has been used for over 50 years,[20] providing a well-established approach for drug delivery. In contrast, studies on MS system require further development.

In contrast, MS-based systems for drug delivery remain under active development, with clinical studies often failing to demonstrate significantly improved therapeutic efficacy[21] and controlled adverse effect.[22] Currently, the only commercially available drug-eluting beads (DEBs), DC Bead LUMI™, represent a relatively recent advancement, with clinical adoption following their commercial introduction around 2017.[22] However, DC Bead LUMI™ is CE-marked only in Europe, and its availability remains geographically limited. Overall, current MS-based platforms remain limited and require further optimization in both material design and drug incorporation, as well as more comprehensive clinical evaluation. Collectively, these challenges highlight that effective and reliable drug-delivery embolic systems have yet to be fully realized and remain an unmet clinical need.

Gel-based embolic systems are at an even earlier stage of development. Currently available gel products, including shear-thinning Obsidio™[23] (2022) and *in situ* gelling Embrace Hydrogel Embolic System[24] (2025) are all non-drug-eluting. To date, no clinically available drug-eluting gel embolic systems exist, and most remain at the research stage. These limitations underscore the need for continued research across material design, drug incorporation, and clinical evaluation to advance these systems toward mature and clinically validated platforms.

This review highlights clinical and recent developments in therapeutic embolic agents with a focus on material innovation and underlying mechanisms. We discuss the design of embolic agents in different forms, including liquid/gel and microsphere (MS), and review strategies for incorporating therapeutic cargos such as chemotherapeutics, immunotherapeutics, and bioactive modulators. We further discuss key design requirements, the current landscape of commercial and experimental agents, and the translational challenges that remain. By bridging advances in materials science, bioengineering, and interventional medicine, we outline how material design is redefining embolization as a multifunctional platform for targeted therapy.

2. Liquid/gel embolic agents for therapeutic applications

2.1. Clinically available liquid embolic agents

Various liquid embolic agents have been applied clinically such as Cyanoacrylates, ethylene vinyl alcohol copolymer, lipiodol, and ethanol. However, their use as therapeutic drug carriers remains limited. The liquid nature enables easier transcatheter delivery compared to other forms of embolic agents but provides less control over deployment and the ability to concurrently deliver a precise therapeutic dose. Thus, liquid embolic agents are regularly used with mechanical embolic agents, such as particles or gelatin sponges, to further block the artery, creating ischemia that enhances the therapeutic effect[25]

2.1.1. Lipiodol. Lipiodol is an iodinated oil-based contrast agent first synthesized in 1901.[26] It has been widely used in clinical practice due to its therapeutic properties, including drug-carrier capability, tumor-selective retention, and a transient embolic effect that further enhances local drug absorption and retention.[27,28]

In 1982, Konno *et al.*[20] first reported the selective accumulation of Lipiodol in hepatocellular carcinoma (HCC) tissues. In this study, Lipiodol served as a carrier for styrene-maleic acid neocarzinostatin (SMANCS), a polymer-conjugated anticancer drug designed with both hydrophilic and hydrophobic properties. This compatibility allowed SMANCS to form a stable suspension when emulsified with Lipiodol, enabling selective tumor targeting. The SMANCS-Lipiodol emulsion was administered intra-arterially to 34 patients at a dosage of approximately 3–4 mg of SMANCS in 3–4 mL Lipiodol per cycle, repeated every 3–4 weeks. Most patients underwent two treatment cycles, resulting in reduced alpha-fetoprotein levels (AFP) for 86% of the patients, and decreased tumor size for 95% cases (reported as a binary outcome).

Another key advantage is the gradual and sustained drug release of Lipiodol-based emulsion, as demonstrated in a

pharmacokinetic study involving five patients.[29] In this study, patients were treated with emulsions containing either doxorubicin (DOX) (40–100 mg) or mitomycin (10–30 mg), both of which are DNA-damaging anticancer agents. To further evaluate clinical efficacy, a study involving 100 HCC patients compared Lipiodol-drug emulsions with gelatin sponge-based drug delivery systems. The Lipiodol group exhibited a markedly higher 3-year survival rate (17.6%) compared to the gelatin sponge group (3.8%). This improvement was attributed to the enhanced stability of the emulsion, which extended the persistence from a few hours to more than 24 hours. This also prolonged intratumoral drug retention and enhanced therapeutic effectiveness through sustained release for up to 27 days.

Although most evidence on Lipiodol's retention comes from pharmacokinetics and tumor uptake studies, recent work by Bannangkoon *et al.*[30] explored its prognostic potential. In a cohort of 124 HCC patients receiving TACE with mitomycin-Lipiodol emulsion, CT imaging revealed four deposition patterns: homogeneous, heterogeneous, defective, and deficient (Fig. 2). Homogeneous accumulation was associated with longer progression-free survival (median 33.2 months) and overall survival (median 54.8 months), while defective patterns correlated with tumor recurrence and poor prognosis.[30]

Despite these benefits, the oily nature of Lipiodol presents limitations for uniform dispersion of hydrophilic drugs. To address this, various emulsion strategies have been developed to improve drug incorporation and stability within the Lipiodol matrix. One approach is to dissolve the hydrophilic drug in a solution with a density similar to Lipiodol, followed by emulsification. For example, SMANCS is a therapeutic agent that targets tumor tissue. It functions by inhibiting DNA synthesis and leading to the apoptosis of cancer cells.[31] In 1984, Kanematsu *et al.*[27] proposed dissolving SMANCS in Urografin, a water-soluble contrast agent that has a comparable density to Lipiodol and subsequently emulsifying. In this clinical study, 13 patients with HCC were treated *via* infusion of this emulsion into the hepatic artery. As a result, 10 patients (~77%) showed marked decreases in alpha-fetoprotein (AFP) levels and reductions in tumor size. Histological evaluation of two of the resected tumor specimens revealed clear signs of tumor necrosis and regression. This emulsification approach proved effective in delivering hydrophilic chemotherapeutic agents to liver tumors and achieving meaningful therapeutic outcomes.

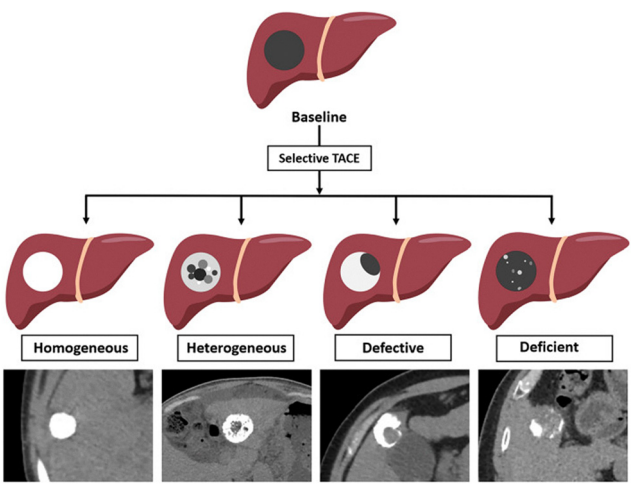

Fig. 2 Diagram illustrates the four Lipiodol accumulation patterns observed on non-enhanced computed tomography. Reproduced from ref. 30, under the terms of the CC BY-NC-ND 4.0 license.

The alternative and more widely adopted method is water-in-oil emulsions, with larger droplets demonstrating better therapeutic efficiency. In 1996, de Baere *et al.*[32] conducted a study on the effect of emulsion properties on therapeutic effectiveness using a rabbit VX2 liver tumor model. In their study, it was found that large-droplet (predominantly 70–100 μm) water-in-oil emulsions achieved superior tumor-targeting efficacy, attaining the highest tumor-to-normal liver uptake ratio of up to 10.26 among all tested formulations. In contrast, small-droplet (predominantly 20–30 μm) oil-in-water emulsions demonstrated undesirable high pulmonary uptake and poor tumor specificity with a tumor-to-normal liver uptake ratio of 4.49. Despite being limited to an animal model, these results provided clear quantitative evidence highlighting the importance of emulsion structure in therapeutic performance.[32]

To further enhance therapeutic effect, Lipiodol, which serves as therapeutic vehicle and transient embolic agent, is routinely followed by particles in clinical practice to achieve effective arterial flow stasis.[1] Studies have also shown that the therapeutic effect can be further enhanced by using particles as drug carrier.[1] For example, compared with conventional TACE (cTACE), which yielded a median progression-free survival (PFS) of 7.0 months and overall survival (OS) of 14.0 months, TACE followed by drug-eluting beads significantly improved outcomes in patients with HCC, extending PFS to 12.0 months and OS to 21.0 months while achieving higher response and disease control rates without increased toxicity.[33] The practice was first proposed by Uchida *et al.*,[25] using gelatin sponge particles after the infusion of the drug-Lipiodol emulsion. Currently, the solid agents include but are not limited to gelatin sponge particles, polyvinyl alcohol (PVA) particles, degradable starch microspheres (DSM), and embospheres.

In a prospective randomized controlled trial,[34] patients with hepatocellular carcinoma were randomized to either lipiodol TACE with cisplatin and gelatin-sponge particles or a control group who did not receive any anti-cancer treatment. The treatment group showed significantly better 1-, 2-, and 3-year survival (57%, 31%, 26%) compared to controls (32%, 11%, 3%). Although survival outcomes (Table 1) after Lipiodol-based TACE vary across studies, there is a consistent trend toward improved patient survival. It is important to account for regional and etiological factors, in addition to chemotherapeutic agent utilized, when comparing across studies.

2.1.2. Ethanol. Ethanol was reported as both an embolic agent and a therapeutic agent in the early 1980s for ablation.[36] It has been mainly used in Japan despite its off-label status, and the guideline was not published until 2016.[37] Ethanol works by disrupting proteins, promoting blood clot formation, and damaging blood vessel walls and surrounding tissues.[37]

Table 1 Summary of clinical trials analysing outcomes with lipiodol-based chemoembolization for treatment of liver cancer. Abbreviations: HCC, hepatocellular carcinoma; SMANCS, styrene-maleic acid neocarzinostatin; AFP, alpha-fetoprotein; PFS, progression-free survival; OS, overall survival

Year	Embolic	Additional anti-tumor drug	Tumor type	Subject	Number of subjects	Outcome measurement	Ref.
1982	Lipiodol	SMANCS ($\sim$1 mg mL^{-1})	HCC	Patients	34	AFP, tumor size	20
1984	Lipiodol-urografin	DOX, Nimustine hydrochloride	HCC	Patients	13	AFP, tumor size, histology	27
1989	Lipiodol, urografin	DOX (40–100 mg); Or mitomycin (10–30 mg)	HCC	Patients	100	Cumulative survival rates: 6 months: 82.0% 1 year: 53.8% 2 years: 33.3% 3 years: 17.6%	29
1990	Lipiodol, gelfoam	Adriamycin (20–60 mg), Cisplatin	HCC	Patients	54	Tumor necrosis, cumulative survival,	25
1996	Lipiodol	N/A	VX2 (rabbit liver tumor	Rabbits	29	Tumor/liver uptake ratio, lung uptake	32
2022	Lipiodol, gelatin sponge	Mitomycin (up to 30 mg)	HCC	Patients	40	OS: 1 y: 57%, 2 y: 31%, 3 y: 26%	35
2024	Lipiodol, gelatin sponge	Mitomycin (10–20 mg)	HCC	Patients	124	PFS: median 33.2 months, OS: median 54.8 months	30

Its ability to penetrate capillary bed[38] and its high occlusion potential[39] make it a powerful embolic agent for permanent occlusion at a capillary level. At the same time, these properties can be dangerous, and the associated risks, including acute and chronic complications and significant morbidity, should be considered.[40] This underscores the necessity of careful use to avoid tissue devitalization and unintended embolization of non-target vascular territories.

Absolute ethanol is commonly mixed with contrast agents to ensure visibility. Lipiodol is the most widely used contrast agent,[41,42] with an ethanol-to-Lipiodol ratio ranging from 1 : 1 to 3 : 1.[37] The emulsification process creates a stable mixture while maintaining ethanol concentration, thereby preserving therapeutic efficacy. Additionally, studies have investigated non-ionic contrast agents such as iohexol. Non-ionic contrast agents have shown a reduced embolic effect compared with Lipiodol-ethanol emulsions, primarily due to the dilution effect.[43] Furthermore, diluted ethanol (50–70%) can be used effectively to treat micro-fistulas, providing a less aggressive option for smaller vascular abnormalities.[43]

Various techniques and materials have been employed to enhance the safety and efficacy of ethanol-based embolization. Balloon occlusion catheters are commonly employed during the procedure to prevent ethanol reflux into non-target areas, thereby minimizing the risk of complications.[41] Coils may be temporarily used to occlude arterial feeders prior to ethanol embolization, ensuring controlled delivery of the embolic agent.[44] Polyvinyl alcohol (PVA) can be mixed with ethanol as a permanent vessel obliterator, providing long-term occlusion.[45]

Ethanol has been used to treat conditions such as slow flow AVM[46,47] due to its ability to directly damage the endothelium of the arteriovenous shunt without capillary bed. High therapeutic efficacy has been reported for ethanol embolization in AVM treatment,[48] with 100% immediate angiographic thrombosis, complete cure in 6 of 8 patients, and no angiographic recurrence at a mean follow-up of 4.2 months. Minor complications occurred in 3 patients, and no procedure-related mortality was reported. However, depending on the location, organ and skin necrosis remain major risks. Thus, despite the well-recognized risks, ethanol remains a highly effective embolic agent for selected AVM cases when applied under carefully controlled conditions.

2.2. Emerging therapeutic liquid/hydrogels based embolic agents

Liquid embolic agents have been widely used in clinical practice for therapeutic purposes. However, their fluid nature can make it difficult to achieve a stable and durable cast at the target site, often requiring combination with particles or coils to ensure durable occlusion.[25] In addition, the oily character of agents like Lipiodol limits their ability to load and release hydrophilic compounds[49] or large molecule therapeutics,[27] restricting their broader application.

To overcome these limitations, recent research has focused on designing gel and liquid embolic agents that integrate embolization with local therapy. Strategies include *in situ* gelling systems such as thermo-responsive and chemically triggered gels; complex coacervates formed *via* phase separation that enable high drug loading with sustained release, and shear-thinning where flow-induced viscosity reduction enables delivery and rapid recovery of solid-like behavior, which ensures localization. This section reviews these advanced gel and liquid platforms that combine embolization with local drug delivery or ablative chemistry (Table 2). In this section, we will review these emerging gel and liquid platforms that couple embolization with local drug delivery or ablative chemistry for therapeutic effects.

2.2.1. Thermo-responsive gels. Thermo-responsive *in situ* gelling systems have been explored as embolic material since mid-1990s.[50] Their sol–gel transition is usually governed by dehydration of hydrophobic polymer blocks, which promotes micelle self-assembly and packing at physiological temperature.[51,52] This thermally driven property allows the formulations to remain as low-viscosity sols at room temperature, facilitating injections through microcatheters, but to form cohesive gels once warmed *in vivo*. The resulting cast conforms to irregular

Table 2 Summary of drug eluting hydrogels under research

Base components	Contrast agent	Drug loaded	Animal studies	Targeted application	Sol–gel transition	Ref.
Pluronic F127, hydroxymethyl cellulose (HPMC), sodium alginate	Iohexol	DOX	Beagle dogs (renal artery embolization), Rabbit VX2 renal tumor models	Renal carcinoma	Thermal-induced gelation at 27 °C	53
p(*N*-isopropyl-acrylamide-*co*-butyl methylacrylate) nanogel	Iohexol	DOX	Normal rabbits (renal artery embolization), Rabbit VX2 liver tumor models	Liver cancer	Thermal-induced gelation at 32 °C	54
Silk elast in like protein polymer (SELP)	Visipaque 320	DOX and sorafenib	Male New Zealand white rabbit hepatic embolization	HCC	Thermal-induced gelation at 37 °C	57,62
Chitosan, β-glycerophosphate (β-GP)	Iopamidol (Isovue® 370)	Sodium Tetradecyl Sulfate (STS)	Canine bilateral iliac aneurysm model	Endoleak treatment after abdominal aortic aneurysm repair	Thermal-induced gelation at 37 °C	66
Chitosan, sodium bicarbonate (NaHCO3), phosphate buffer (PB)	Visipaque 320 (VIS)	Doxycycline	Pig renal arteries	Endoleak prevention/treatment after EVAR	Thermal-induced gelation at 37 °C	65
Gelatin, oxidized dextran (O-Dex), ionic liquid (IL)	Iohexol	Ionic liquid (antimicrobial agent	Porcine perianal fistula model, Rat subcutaneous implantation	Enterocutaneous fistula treatment	Chemical cross-linking (imine bonds)	67
Quaternized chitosan (QCS), gum arabic (GA)	Iohexol	DOX	New Zealand rabbits (renal artery, ear VX2 tumor, liver orthotopic VX2 tumor)	Tumor chemoembolization	Liquid–liquid phase separation (electrostatic interactions)	70
Silk fibroin proteins, nanoclay (NC) particles	Iohexol	BSA, ICG, Nivolumab	Porcine renal survival model, Rat femoral artery model	vascular diseases/ tumors	Shear induced	75
Gelatin, LAPONITE® nanoclay		DOX, anti-PD-1 (aPD-1)	Mouse liver tumor model (Hepa 1-6 cells)	TACE for HCC	Shear induced	76
Raltitrexed, kaempferol, and tantalum nanoparticles	Tantalum nanoparticles	Raltitrexed and kaempferol	Rabbit VX2 ear artery tumor model, a mouse H22 subcutaneous HCC model, and a rat N1-S1 orthotopic HCC model	HCC, ear artery tumor	Shear induced	79

lumens and distal branches, thereby improving embolic precision, limiting reflux and washout, and enhancing occlusion stability and therapeutic efficacy.

One of the most widely used thermal responsive materials is Pluronic F127 (F127), which undergoes a sol–gel transition near 37 °C (Fig. 3A). This property aligns with physiological temperature, allowing delivery as a low viscosity liquid that rapidly transforms into a gel *in situ*. However, F127 gels alone are mechanically weak and susceptible to erosion.[51] Thus, F127 is usually blended with other polymers to reinforce the network. For example, He *et al.*[53] blended F127 with hydroxymethyl cellulose (HPMC) and sodium alginate to strengthen the matrix. DOX was loaded for chemotherapy along with iohexol for X-ray imageability. This formulation achieved complete renal artery occlusion in beagle models within 10 minutes and produced marked tissue necrosis by 2 weeks. In rabbit VX2 renal tumors, transarterial chemoembolization with the DOX-loaded gel induced vessel occlusion, tumor necrosis, and high apoptosis, confirming its combined embolic and chemotherapeutic activity.

Another widely studied thermoresponsive material is poly(*N*-isopropylacrylamide), commonly abbreviated PNIPAm, which undergoes a sol–gel transition near 32 °C. Because this transition temperature is below physiological temperature,

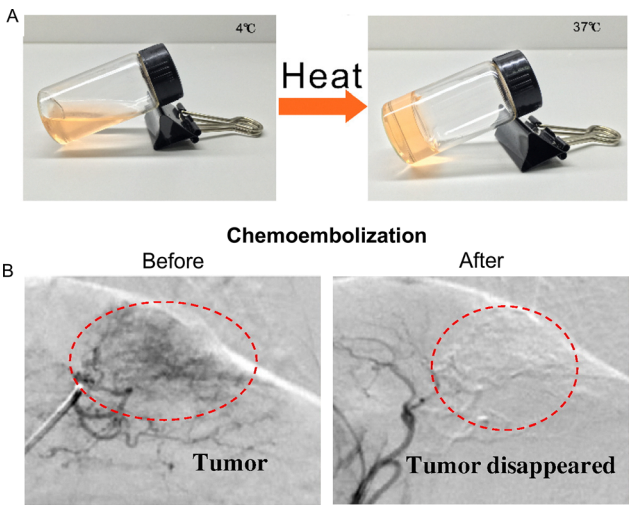

Fig. 3 (A) Sol–gel transition of DOX-loaded temperature sensitive hydrogel. (A) is reproduced with permission from ref. 53. Copyright 2020, Elsevier. (B) Angiography (DSA) of rabbit VX2 liver tumor before and after treatments of intra-arterial infusion with TACE with IBi dispersion. Iohexol (350 mg I mL^{-1}) was used as a blood-vessel contrast for DSA images. (B) Reproduced with permission from ref. 54. Copyright 2015, Elsevier.

unmodified PNIPAm gels too early, raising the risk of premature solidification and catheter clogging during delivery. To address this limitation, PNIPAm can be copolymerized with hydrophobic monomers such as butyl methacrylate (BMA), typically in the presence of a crosslinker and stabilizing agents.[54,55] The incorporation of BMA disrupts polymer–water hydrogen bonding and strengthens hydrophobic interactions, thereby shifting the transition upward to approximately 37 °C. Importantly, this modification sharpens the gel transition, ensuring that the system remains injectable at room temperature but gels rapidly and completely at physiological temperature, which improves delivery safety and on-target solidification.[56]

Qian *et al.*[54] developed DOX-loaded PNIPAm-BMA nanogels dispersed with iohexol (IBi-D) for TACE. The system exhibited a sol–gel transition point of 37 °C. It displayed a pH-sensitive release profile, where only ~5–6% of DOX was released over 7 days at neutral pH, while ~28% was released under acidic tumor-like conditions, and the presence of surfactant further accelerated release to ~87%. In the rabbit renal arteries, IBi-D showed clear dose-dependence embolization. A low dose of 0.5 mL mainly occluded peripheral arteries, whereas increasing the dose to 2 mL resulted in complete blockage of peripheral, small, and large arteries. In rabbit VX2 liver tumors, transarterial chemoembolization with IBi-D resulted in complete arterial occlusion with controlled intratumoral DOX delivery. The authors reported that tumors treated with IBi-D grew at a rate approximately four times lower than those treated with free DOX (TAC) or embolic-only therapy (TAE) (Fig. 3B). Overall, the formulation combined thermos-responsive cast formation, radiopacity, and pH-tuned chemotherapy in a catheter-deliverable format.

Recently, silk elastinlike protein polymers (SELPs) have been developed as thermosensitive gelling polymers that are injectable as low-viscosity fluid at room temperature and undergo *in situ* gelation to form solid hydrogels at physiological temperature (37 °C).[57] Owing to their tunable network structure and biocompatibility, SELPs have been explored as delivery platforms for a broad range of therapeutic payloads, including cells,[58] adenoviral genes,[59] plasmid DNA,[60] proteins,[61] chemotherapeutics *etc.* Poursaid *et al.* developed an *in situ* gelling SELP formulation (SELP-815K) for chemoembolization of HCC.[57] By tuning the relative lengths of silk and elastin blocks in the polymer, the polymer was formulated at 12 wt% and processed under shear to achieve a low viscosity (<150 cP), enabling catheter injectability, rapid gelation (<5 min) for local fixation, and a high storage modulus ($>1 \times 10^5$ Pa) sufficient for arterial occlusion. An *in vitro* occlusion model designed to simulate TACE procedure demonstrated a marked increase in the systemic pressure from 1 psi (pre-embolization) to 4 psi (post-embolization). This indicated effective vessel occlusion by the SELP-815K gel. In an *in vivo* hepatic embolization study in male New Zealand White rabbits, SELP-815K gel was injected proximally at the left and right hepatic artery branch points. Angiographic and fluoroscopic imaging before and after injection clearly identified the point of vascular stasis. Histological analysis of the hepatic tissue also identified the SELP-815K within hepatic arterioles, and within associated lymphatic vessels. Vacuolization in the hepatocytes was also observed, indicating a decreased blood supply to the liver cells.[57] Expanding this work, HCC therapeutic drugs namely sorafenib and DOX were incorporated into the SELP-815K polymer. Drug incorporation had no significant effect on viscosity, gelation kinetics and gel stiffness of the embolic agent. The gel had a single drug loading of 25 mg mL^{-1} and 50 mg mL^{-1}, and dual drug loading of 25 mg mL^{-1} of each drug yielding a total drug loading of 50 mg mL^{-1}. The release profile was evaluated for 30 days *in vitro*. For dual drug loaded gels, 30% of the total drug content of the DOX and sorafenib was released after 30 days. Interestingly, dual-drug loaded gels exhibited significant increase in cumulative release over the 50 mg mL^{-1} single drug loaded gels.[62]

In a separate study on SELP-815K, Poursaid *et al.*[63] demonstrated that the chemical and physical form influence the injectability and release kinetics. For both doxorubicin HCl, sorafenib tosylate or base forms dissolved in dimethyl sulfoxide (DMSO), drug incorporation increased the viscosity of the SELP solution beyond the 150 cP injectability threshold. In contrast, formulations incorporated either drug in base form (milled powder) preserved the rheological behavior and gelation kinetics of SELP, thereby maintaining catheter injectability. Drug distribution studies showed that DMSO-dissolved drugs achieved more homogeneous dispersion within the polymer matrix, whereas milled drugs formed hydrophobic clusters within the polymer network. Despite this heterogeneous distribution, milled formulations exhibited more sustained release profiles, particularly for sorafenib, which showed slower cumulative release due to hydrophobic interactions with the SELP matrix. *In vitro* release studies using 12% SELP gels demonstrated therapeutically relevant concentrations of DOX for HepG2 cells (IC_{50} of 0.62 ± 0.41 μM) for at least 14 days and sorafenib for up to 30 days (IC_{50} of 1.72 ± 0.7 μM). Notably, the presence of DOX significantly enhanced sorafenib release in dual-drug formulations by day 7, where dual-loaded sorafenib released 2.1 ± 0.3 μM compared to 0.7 ± 0.2 μM in the single-drug gels. These findings suggest that complementary drug-polymer and drug-drug interactions within the gel matrix effectively modulate the delivery profile.

2.2.2. Chemically triggered gels. Chemically triggered hydrogels undergo sol–gel transition or network formation in response to chemical changes in their environment. These changes may include pH or ionic shifts, which alter polymer protonation and solubility, or covalent reactions such as Schiff base crosslinking between aldehyde and amine groups. In the context of embolization, such mechanisms allow the materials to be injected as liquids and then solidify *in situ* under physiological conditions. Beyond simple vascular blockage, chemically triggered systems are often designed to deliver additional therapeutic functions, such as endothelial ablation, inhibition of matrix metalloproteinases, or tissue adhesion, thereby improving occlusion stability and reducing recurrence.

Chitosan-based hydrogel has been adapted as chemically triggered embolics with added sclerosants to achieve therapeutic

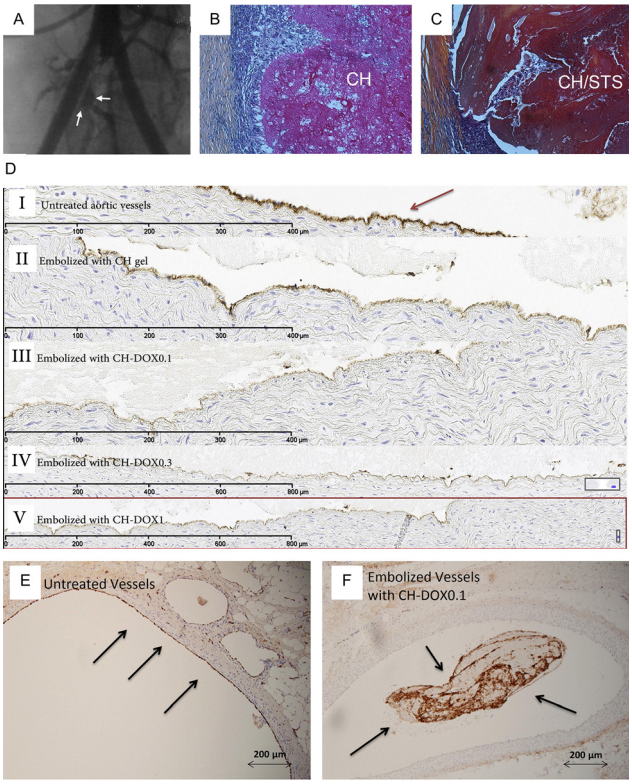

Fig. 4 Embolization of CH and CH/STS gels in a canine bilateral aneurysm model of EVAR. (A). Angiography at 3 months with a significant type I endoleak on a CH-embolized aneurysm (arrows). (B) and (C) Histopathology showing the persistence of CH and CH/STS blocs at 3 months. Cell infiltration within the material was observed on both cases. However, inflammation was more intense around CH/STS (HPS staining). (A), (B) and (C) are reproduced with permission from ref. 66. Copyright 2012, Elsevier. (D). Factor VIII immunostaining of aortic vessels: (I) untreated or embolized *ex vivo* with (II) CH gel; (III) CH-DOX0.1 gel; (IV) CH-DOX0.3 gel; (V) CH-DOX1 gel. Endothelial cells (Arrow, brown staining) are present at the lumen of untreated artery and still partially present after embolization by CH gel but absent after embolization with DOX-containing CH gels. Factor VIII immunostaining of *in vivo* embolized vessels: (E) untreated; (F) embolized with CH-DOX0.1. The figure shows that the endothelial lining is removed *in vivo* after embolization with CH-DOX0.1 gels, while it is clearly visible on untreated arteries (brown stain, arrows). (D), (E) and (F) are reproduced with permission from ref. 65. Copyright 2017, Elsevier.

effect. Fatimi *et al.*[64] mixed chitosan with β-glycerophosphate as a gelling agent, iopamidol for radiopacity, and sodium tetradecyl sulfate (STS) as a detergent-based sclerosant for treating abdominal aortic aneurysm endoleaks. The increase in STS content accelerated gelation and strengthened the gels (storage modulus up to ∼1357 Pa at 3% STS) and induced endothelial denudation in *ex vivo* canine arteries. In a bilateral iliac aneurysm dog model, aneurysms treated with chitosan/STS gels showed no endoleaks after three months, whereas those treated with chitosan alone developed leaks (Fig. 4A). Histopathological analysis of the explanted aneurysm specimen confirmed that the CH and CH/STS gels were present en bloc. (Fig. 4B and C). Despite ongoing degradation, the CH gel exhibited cell infiltration, and portions of the gel were surrounded by fibrous tissue. (Fig. 4B). The CH/STS material exhibited poor healing and appeared less porous. Strong inflammatory responses, including macrophages and numerous polymorphonuclear (PMN) cells, indicated acute inflammation, particularly around CH/STS (Fig. 4C).

Building on this concept, Zehtabi *et al.*[65] added sodium bicarbonate as a second gelling agent to gradually raise pH and deprotonate chitosan amine groups to further support ion-triggered gelation. Doxycycline was introduced as the therapeutic component, replacing STS, while iopamidol again provided radiopacity. The doxycycline release followed a two-stage profile. First, there is a burst release within the first 24 hours, ∼85% doxycycline release for gel with 1% w/v doxycycline content and ∼60% doxycycline release for gel with 0.1% w/v doxycycline content. This first release promoted endothelial sclerosis and ablation. Then, a slower release continued for up to 7 days. The kinetic parameters calculated from Korsmeyer–Peppas formula were $n = 0.89$ ($k = 4.5$) for 1% w/v doxycycline in gel, and $n = 0.96$ ($k = 1.81$) for 0.1% w/v doxycycline content gel, indicating controlled release close to zero order kinetics. This helped inhibit matrix metalloproteinases (MMPs) and reduced the risk of vessel wall degradation and recanalization. The gels showed suitable mechanical properties for embolization, with storage moduli >800 Pa and resistance high perfusion pressures greater than 200 mmHg. *Ex vivo*, chitosan-only gel had a little effect on the endothelium (Fig. 4D(II)), whereas doxycycline loaded gels effectively removed the endothelial lining (Fig. 4D(III–V)). *In vivo* studies in pig renal caudal polar artery model demonstrated high embolization success (96% immediate, 86% after 20 min) and good radiopacity. Factor VIII immunostaining of embolized artery exhibited removal of endothelial lining by the doxycycline loaded chitosan gel (Fig. 4F) whereas a stable endothelium was observed for untreated vessels (Fig. 4E).

Tissue-adhesive hydrogels represent another chemically triggered strategy for therapeutic embolization. These systems form strong and stable bonds with surrounding tissues, which help secure the embolic cast, reduce reflux and migration, and promote local healing. Adhesion is generally achieved through two complementary mechanisms. Covalent coupling occurs when reactive groups, such as aldehydes in oxidized dextran, form Schiff base bonds with tissue amines. Noncovalent interactions, like hydrogen bonding, contribute additional adhesion even when covalent bonding is incomplete. These bonds allow hydrogels to anchor firmly to wet and irregular tissue surfaces, enhancing cast stability.

In 2025, Kim *et al.*[67] developed a tissue-adhesive system for enterocutaneous fistula closure. The system was based on a gelatin-oxidized dextran matrix, where Schiff base crosslinking occurred both internally and with tissue proteins. A choline- and geranate- based ionic liquid were incorporated to reinforce mechanical properties and provide intrinsic antimicrobial activity, while iohexol was added for radiopacity. The optimized formulation exhibited high elasticity (storage modulus >4000 Pa) and recoverability. The gel also exhibited excellent adhesive properties with explanted porcine skin where it withstood all mechanical challenges including stretching, bending, twisting,

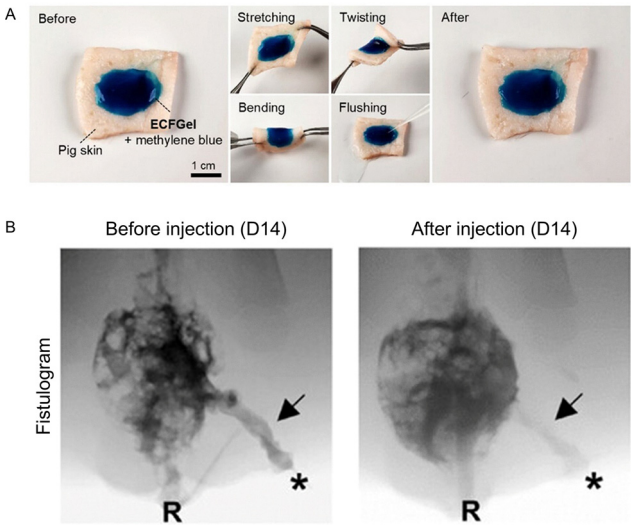

Fig. 5 (A). Images illustrating ECFGel's tissue adhesiveness on pig skin and resistance against various mechanical challenges. (B). Fistulogram at D14 before and after injecting ECFGel into the fistula tract, confirming successful occlusion of the tract with ECFGel. Asterisks indicate the outer opening, "R" denotes the rectum, and arrows point to the fistula tract. (A) and (B) are reproduced with permission from ref. 67. Copyright 2025, John Wiley and Sons.

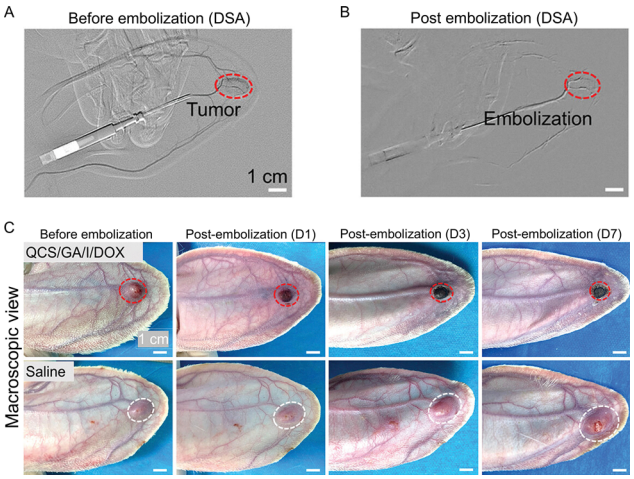

Fig. 6 Rabbit ear VX2 tumor chemoembolization with QCS/GA/I/DOX complex coacervate. (A) DSA images of the central auricular artery before embolization. (B) DSA image of QCS/GA/I/DOX complex coacervate (red arrow) post-embolization. (C) Macroscopic view of the rabbit ear VX2 tumors before and post-embolization with QCS/GA/I/DOX complex coacervate and saline. (A), (B) and (C) are reproduced with permission from ref. 70. Copyright 2024, John Wiley and Sons.

and water flushing, indicating its potential to durably occlude enterocutaneous fistula tracts without detachment or fracture (Fig. 5A). In porcine perianal fistula models, the hydrogel was delivered under fluoroscopic guidance and successfully occluded fistula tracts, promoting tissue healing. Pre-injection fistulography identified a distinct tract extending from the perianal skin to the rectum, whereas post-injection imaging confirmed complete occlusion of the fistula (Fig. 5B). Histology confirmed accelerated healing, with increased deposition of type I collagen, reduced bacterial burden (7–44 folds lower than untreated), and enhanced cellular proliferation and vascularization. Compared to the chitosan-sclerosant systems, which rely on endothelial ablation and MMP inhibition, this adhesive hydrogel exerted its therapeutic effect through a combination of mechanical sealing, antimicrobial protection, and pro-healing activity.

2.2.3. Complex coacervates gels. Complex coacervation occurs when two oppositely charged macromolecules are mixed in water. Driven by electrostatic interactions and counterion release, the solution spontaneously separates into a dilute, polymer-poor phase and a dense, polymer-rich phase called the coacervate.[68] The injectability of coacervates for embolization arises from their reversible ionic interactions, which allow flow under shear. Once delivered, these interactions reform to create a dense, cohesive phase that resists washout and stabilizes the embolic cast.

Complex coacervates have been shown to achieve distal embolization, durable occlusion, and sustained chemotherapy within a catheter-deliverable format, addressing key limitations of Lipiodol and particle-based systems. Liu *et al.*[69] developed a complex coacervate for TACE using quaternized chitosan (QCS) and gum arabic (GA), with iohexol (I) added for radiopacity and DOX for chemotherapy. The formulation with 30% iohexol achieved comparable imageability to Lipiodol, while providing higher drug loading efficiency (96%) and sustainable release over 35 days in contrast to the rapid burst release of Lipiodol emulsions. Rheological testing showed shear-thinning behavior, allowing smooth delivery through clinical microcatheters ($\leq$1.7 F) with injection forces below 50 N. In rabbit VX2 tumor mode, the QCS/GA/I/DOX coacervate achieved complete embolization of the central auricular artery and its branches and formed a stable cast without fragmentation and migration (Fig. 6A and B) Tumors embolized with QCS/GA/I/DOX coacervate gradually underwent ischemic necrosis and its volume was significantly reduced over time (Fig. 6C). Histological analysis confirmed coacervate deposition in distal branches' diameters of 16 μm, which was associated with shrinkage of glomeruli and tubules. These findings correlated with significant tumor regression and, importantly, occurred without formulation-induced ischemic necrosis. Contrast-enhanced ultrasound confirmed complete perfusion loss, while histology demonstrated coacervate distribution into vessels as small as 16–20 μm, a penetration depth superior to that achieved by commercial MSs ($>$125 μm).[42]

2.2.4. Shear-thinning nanocomposite gels (mechanical trigger). Shear-thinning gels exhibit decreased viscosity when exposed to shear stress but recover their solid-like behavior once the stress is removed.[71,72] This property allows them to be injected as a fluid through microcatheters and then regain stability to form a solid-like durable occlusion once delivered. The behavior is governed by dynamic and reversible crosslinks such as hydrogen bonding, electrostatic interactions, π–π stacking, polymer chain entanglement, particle–particle interactions, and polymer-particle interactions, which are disrupted under shear and reformed after delivery to stabilize the embolic cast.[73,74]

Unlike *in situ* gelling or phase-separating systems, shear-thinning embolic materials rely on rheological behavior to enable injectability and localization, without requiring a distinct chemical or thermal phase transition. Complex coacervates described in Section 3.1.3 can also display shear-thinning behavior. However, they are not typically classified as shear-thinning systems because their primary identity lies in ionic complexation that drives liquid–liquid phase separation. In contrast, shear-thinning nanocomposite gels are explicitly designed around reversible networks that rely on shear disruption and recovery. For this reason, despite some overlapping rheological features, coacervates and nanocomposite gels are discussed in separate sections.[75]

Hu *et al.*[75] developed a silk-fibroin nanoclay embolic material (SEM) in which noncovalent electrostatic interactions provided shear-thinning behavior. The molecular weight of silk fibroin was tuned by adjusting degumming time during silk cocoon processing, which in turn modulated rheological properties. The resulting gels displayed solid-like mechanics with rapid recovery after shear and could be readily delivered through clinical microcatheters. When supplemented with Omnipaque (iohexol), the formulations also became radiopaque, allowing clear visualization under fluoroscopy, CT, and MRI. Beyond mechanics, SEMs were engineered for multifunctional therapy. The gels co-loaded Indocyanine Green (ICG) and Alexa-594 BSA as imaging probes, and nivolumab (Nivo), an immune checkpoint inhibitor. *In vitro*, Nivo showed sustained release (~6% over 28 days), indicating compatibility with large biologics. In a porcine renal artery model, SEM-Nivo-ICG achieved persistent embolization with strong radiographic visibility. Importantly, SEM-I-BSA-ICG-treated kidneys exhibited strong arterial BSA-Alexa fluorescence at day 0, whereas by day 14, the signal had shifted to the renal parenchyma and interstitial space (Fig. 7A), indicating successful protein delivery. ICG also remained arterial at day 0 but showed markedly reduced fluorescence at D14 (Fig. 7A). Additionally, histology revealed that BSA-Alexa remained intravascular when the IEM was intact whereas when the IEM was disrupted, the tracer leaked into surrounding tissue (Fig. 7B). Fluorescence imaging detected BSA-Alexa in the renal cortex (Fig. 7C), confirming its peripheral localization compared to controls. The combination of tissue ischemia (kidney) and targeted delivery to the renal cortex *via* SEM-I embolization offers a dual approach for minimally invasive oncologic therapy. By first disrupting the vascular endothelium barrier with embolization and then releasing the drug into adjacent parenchyma, this method may overcome transport limitations. Similarly, Nivo delivery *via* SEM-I-Nivo-ICG was assessed. Two weeks post-embolization, immunohistochemistry showed high Nivo levels in both the embolized arteries and surrounding parenchyma (Fig. 7D), confirming successful delivery to the renal cortex. IHC confirmed that Nivo localized both the embolized arteries and surrounding parenchyma, reaching ~35-fold higher local concentrations compared with intravenous dosing, without systemic toxicity. These results highlight a novel, localized approach for sustained immunotherapy delivery directly to tumor tissue, reducing systemic side effects and improving response rates in solid tumors. This gel-embolic platform could also lower healthcare costs and improve patient quality of life.

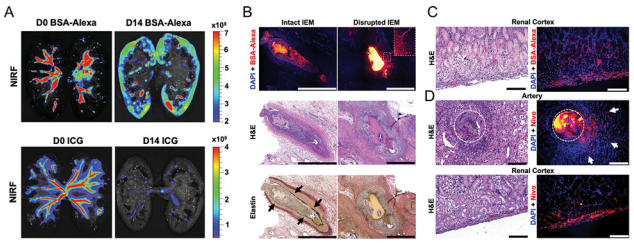

Fig. 7 (A) NIRF imaging of BSA-Alexa and ICG distribution in the bisected kidneys at D0 and D14 post-SEM-I-BSA-ICG embolization. Comparison of BSA-Alexa and ICG signal, respectively, in NIRF imaging at the renal cortex D0 and D14 (n = 4). (B) Representative BSA-Alexa fluorescence imaging (red), H&E, and elastin stains in arteries with intact elastic membrane (IEM; arrow) and disrupted IEM. BSA-Alexa was detected outside of the artery in the interstitial space in arteries with disrupted IEM (white dotted box), not from the artery with intact IEM (black arrows). (C) Representative H&E image and BSA-Alexa fluorescence imaging (red) at the renal cortex of SEM-I-BSA-ICG embolized kidney at D14, showing the successful delivery of BSA-Alexa (red) to the renal cortex. D. Representative H&E and IHC staining of Nivo at D14 post-SEM-I-Nivo-ICG embolization, showing successful delivery of Nivo outside of an artery (arrow) and its presence at the renal cortex. (A), (B), (C) and (D) are reproduced with permission from ref. 75. Copyright 2021, John Wiley and Sons.

A gelatin-LAPONITE® nanoclay shear-thinning hydrogel carrying DOX and the immune checkpoint inhibitor aPD-1 was developed for HCC.[76] The reversible interactions among nanoclay and gelatin particles provided the gels with solid-like mechanics, rapid recovery, and comfortable injectability (<35 N). The authors proposed that electrostatic interaction-controlled DOX release, leading to increased release under acidic conditions (~70% at 10 days), while aPD-1 release was governed by diffusion, desorption, and matrix degradation, resulting in higher release at neutral pH (~85% at 10 days). *In vitro*, DOX alone induced modest cytotoxicity in HepG2 cells, but DOX treatment upregulated PD-L1 on tumor cells after 7 days, enhancing tumor responsiveness to aPD-1 therapy. This mechanistic synergy supported the rationale for co-delivery of DOX and aPD-1 within one embolic platform. *In vivo*, a mouse liver tumor model showed that the DOX + aPD-1embolic gel resulted in smaller residual tumor size, greater apoptotic tumor cell death, and enhanced infiltration of cytotoxic T cells (Fig. 8A and B). Histology and immunofluorescence confirmed increased apoptosis and immune activation, supporting the potential of shear-thinning nanocomposites as dual chemo-immune embolization platforms (Fig. 8C).

Raltitrexed is a chemotherapeutic drug used in the treatment of colorectal cancer. It is administered as an aqueous solution *via* intravenous infusion, and its clinical use has been established primarily in Europe.[77] More recently, there has been emerging interest in incorporating raltitrexed into localized delivery systems. In a novel approach, raltitrexed forms a supramolecular hydrogel in water under ultrasonic irradiation. In 2021, Qian *et al.*[78] used ultrasonication promote molecular dispersion and facilitates subsequent self-assembly, which is

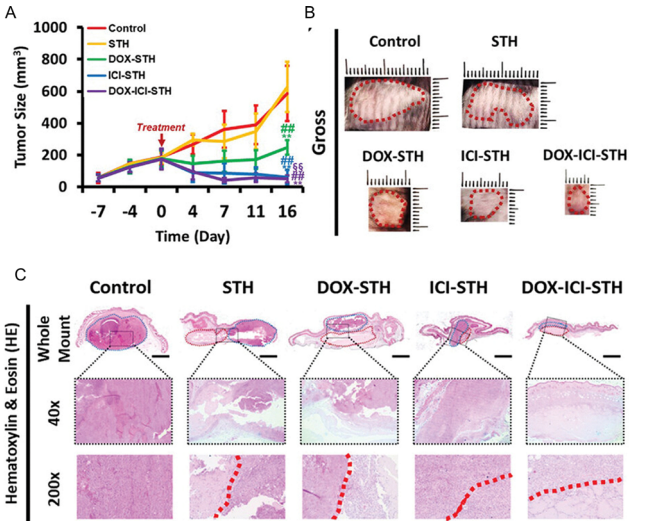

Fig. 8 (A) Tumor growth curve of DESTH treatments in Hepa 1-6 mouse tumor model. *$p < 0.05$, **$p < 0.01$, ANOVA (*: compared to control, #: compared to STH, and §: compared to DOX-STH). B. Endpoint tumor gross images of experimental groups. The red dotted line: tumor. (C) Histopathological analysis of Hepa 1-6 mouse tumor models treated with DESTHs (DOX, ICI, DOX-ICI). Blue dotted line in the whole mount: tumor, red dotted line in the whole mount: STH remnant. The red dotted line in 200×: the border between the tumor and STH. Scale bar is 2 mm, 500, and 100 μm for whole mount, 40×, and 200×, respectively. (A), (B) and (C) are reproduced with permission from ref. 76. Copyright 2023, John Wiley and Sons.

governed by non-covalent interactions, primarily hydrogen bonding and π–π stacking. These interactions drive the formation of nanofibrous structures that further intertwine into a three-dimensional network.

In 2025, Peng *et al.*[79] further developed the raltitrexed gel system by incorporating kaempferol, a clinically used chemotherapeutic drug, and tantalum nanoparticles as an X-ray contrast agent. In this system, kaempferol reinforces mechanical strength through additional hydrogen bonding and π–π stacking with raltitrexed, and tantalum nanoparticles are physically embedded within this network. *In vitro* drug release studies conducted at pH 7.0 and 5.5 over 720 hours demonstrated pH-responsive and sustained release for raltitrexed, kaempferol, and tantalum nanoparticles, with accelerated release under acidic tumor microenvironment conditions. *In vivo* evaluation spanned rabbit and rat renal artery embolization models, a rabbit VX2 ear artery tumor model, a mouse H22 subcutaneous HCC model, and a rat N1–S1 orthotopic HCC model. Raltitrexed gel achieved complete macrovascular and microvascular occlusion with negligible recanalization, confirmed by DSA and CT imaging. When combined with radiotherapy, raltitrexed gel demonstrated superior tumor suppression across all models, with tumor volume in the orthotopic HCC group decreasing below baseline over 14 days while radiation alone failed to arrest tumor progression. Key mechanistic findings included tantalum nanoparticles mediated radiosensitization *via* elevated ROS and γ-H2AX expression, kaempferol-mediated downregulation of HIF-1α and VEGF, and robust induction of immunogenic cell death evidenced by CRT exposure, HMGB-1 release, and ATP secretion. These effects collectively promoted dendritic cell maturation, CD^{8+} T cell infiltration, and a shift from immunosuppression to immunoactivation, with no significant systemic toxicity.

3. MS-based embolization by drug class

Drug-eluting MSs (DEMs), also known as drug-eluting beads (DEBs), are MS-based therapeutic agents that provide simultaneous vascular occlusion and localized drug release.[80] This strategy enables high intratumoral drug concentrations with reduced systemic toxicity. Over time, these MSs have been designed to carry and deliver a wide variety of therapeutic agents, from conventional chemotherapeutics to modern targeted drugs. They differ in the types of drugs incorporated into DEMs, the polymer materials used for MS fabrication, and the mechanisms governing drug loading and release.

DEMs were initially developed to deliver cytotoxic chemotherapy agents for TACE.[81] In Europe, several MS systems have received CE marking (European conformity certification that permits marketing within the European Economic Area) for use with specific chemotherapeutic agents such as DOX and irinotecan. Notable examples include DC Bead™ and DC Bead LUMI™ (Boston Scientific, USA), Embozene TANDEM™ (Varian Medical Systems Inc., USA), HepaSphere™ (Merit Medical Systems, USA), and LifePearl® and BioPearl® (Terumo European Interventional Systems, Belgium).[80] Although significant progress has been demonstrated in both *in vitro* and *in vivo* studies, broader clinical adoption remains limited, and further research is needed to optimize therapeutic outcomes. In the United States, no MS product has yet received U.S. Food and Drug Administration (FDA) approval as a drug-eluting device.[80]

In this section, DEMs are discussed according to the therapeutic class of the incorporated drug, as most systems share similar hydrogel compositions and drug-loading mechanisms. Both clinically approved and experimental systems are included, and each category is analyzed with respect to its drug-loading and release mechanisms, polymer composition, and therapeutic applications across various cancers.

3.1. Cytotoxic chemotherapeutic agents

Cytotoxic chemotherapeutic agents, such as anthracyclines and topoisomerase inhibitors, remain a cornerstone in cancer treatment. Most of these drugs induce cytotoxicity by targeting DNA or microtubule structures, disrupting DNA replication or mitotic processes and ultimately inducing apoptosis.[82] To enhance therapeutic efficacy and reduce drug resistance, cytotoxic agents are often administered in combination regimens.[82] Nevertheless, treatment resistance and tumor relapses remain major clinical challenges.[82]

3.1.1. Commercially available DEM. A common mechanism that DEMs used for cytotoxic chemotherapy in TACE operate through is ion-exchange loading of cationic chemotherapeutics

onto anionic hydrogel matrices, followed by diffusion-controlled release within embolized vessels. These systems are generally composed of non-biodegradable hydrogels functionalized with negatively charged groups, such as sulfonate or carboxylate moieties, which enable electrostatic binding and gradual eluting of positively charged drugs.[83] Polymer composition and cross-linking density play crucial roles in governing both drug-loading efficiency and release kinetics.

Among the existing systems, sulfonate-modified Polyvinyl alcohol (PVA) MSs are the most widely used in clinical practice.[84] A representative example is DC Bead™, a PVA MS modified with 2-acrylamido-2-methylpropanesulfonate (AMPS).[85,86] The incorporation of sulfonate groups enables ionic loading of cationic drugs such as DOX (Fig. 9 A and B), where positively charged DOX hydrochloride exchanges with counter-ions bound to the sulfonate sites.[87,88] DC Bead™ can load up to 45 mg DOX per mL of MSs[89] or 50 mg mL^{-1} of irinotecan,[90] a topoisomerase-I inhibitor. It can achieve controlled release over weeks. Besides, drug loading causes changes in MS diameter (Fig. 9C). During loading, larger MSs (700–900 μm) contracted by approximately 35% in mean diameter at maximum loading capacity, whereas the smaller MSs (100–300 μm) demonstrated markedly minimal shrinkage under the same conditions.[89] Following drug release, the MS remained in place as a permanent embolic. This durable occlusion, combined with slow diffusion-driven drug elution (less than 20% of DOX eluted within 24 hours from DC Bead™ compared to 100% eluted within 4 hours from lipiodol emulsion),[89] achieved high local drug concentration and prolonged tumor exposure while minimizing systemic levels. Research[91] shows that DC Bead LUMI™ has a higher doxorubicin loading capacity of 205 ± 4 mg mL^{-1} compared with LC Bead™ (also known as DC Bead™ in the US) (45 mg mL^{-1}) and therefore exhibits a higher drug release amount (Fig. 9 C) under similar conditions. A phase I/II trial[92] showed the safety and efficacy of DOX-eluting beads (DEB, Biocompatibles UK, London, UK) which is a safe and effective treatment for HCC (Fig. 9 D, E, and F) without systemic toxicity. Other PVA-sulfonate products include CalliSpheres® (Jiangsu Hengrui Medicine Co., Ltd, Jiangsu, China), a DEM similar in composition (a PVA macromer) to DC Bead™.[93]

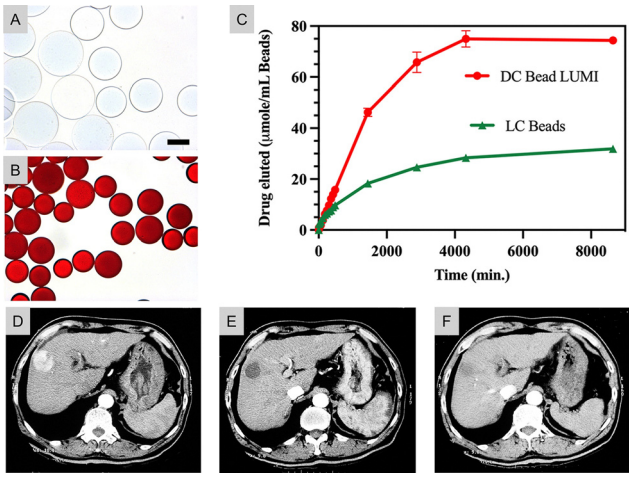

Fig. 9 (A) and (B): LC beads before (A) and after (B) loading of DOX;[91] (C): time-dependent release profiles of DOX from DC Bead LUMI (74.4 ± 0.5 μmol Dox per mL) compared with LC Bead (31.9 ± 0.3 μmol Dox per mL). Data are shown as mean ± SD (n = 3).[91] (A), (B), and (C) are reproduced with permission from ref. 91. Copyright 2022, Springer Nature. (D), (E), and (F): contrast-enhanced CT images from a patient demonstrating a complete response based on the modified Response Evaluation Criteria in Solid Tumors (mRECIST).[92] (D) Baseline CT showing a 4 cm hypervascular tumor prior to therapy. (E) CT at 1 month following the second DEB-TACE session indicating complete necrosis with decreased tumor size. (F) CT at 4 months post-treatment confirming complete necrosis and additional shrinkage of the tumor. (D), (E), and (F) are reproduced with permission from ref. 92. Copyright 2007, Elsevier.

Recent commercial MSs have introduced alternative polymers and designs. HepaSphere™/QuadraSphere® (Merit Medical) uses a sodium acrylate–vinyl alcohol copolymer MS that is supplied desiccated and expands around 4 times upon hydration.[94,95] HepaSphere™ MSs can be loaded with DOX; however, studies have found that their drug uptake and release are less uniform compared with DC Bead, exhibiting more rapid release and occasional MS fragmentation.[96] This is attributed to differences in polymer crosslinking and ionic content: HepaSphere™'s poly(acrylate) carries fewer fixed charges than AMPS-rich PVA, resulting in weaker drug binding and a faster initial burst release (in one report, 75% of loaded idarubicin was released in ~42 minutes from HepaSphere™ *vs.* ~24 minutes for DC Bead and >90 minutes for certain newer MSs).[97]

Tandem® (Embozene-TANDEM) MSs (Varian) represent a core–shell design: a polymethacrylate-based hydrogel core capable of drug loading, coated with an ultrathin Polyzene-F® (polyphosphazene) outer layer for biocompatibility and size precision.[98,99] Tandem's tight size distribution (104.8 ± 6.8 μm after loading of DOX)[100] and non-swellable hydrophobic coating improve predictable catheter delivery and may slow drug diffusion out of the core, contributing to more prolonged release profiles (*e.g.* Tandem showed the slowest idarubicin elution *in vitro* among tested MSs).[97]

LifePearl™ (Terumo) is composed of a polyethylene glycol (PEG) hydrogel network co-polymerized with 3-sulfopropyl acrylate (a sulfonic acid monomer).[101] This PEG-based MS similarly binds DOX or irinotecan *via* sulfonate groups, but the PEG matrix and rigorous calibration yield higher drug loading concentration compared to DC Bead, HepaSphere™, and Tandem[97] and better handling (*e.g.* longer suspension stability in syringes) compared to DC Bead and HepaSphere™.[99] Across these commercial DEMs, differences in polymer charge density, porosity, and mechanical compliance largely dictate therapeutic behavior. Highly charged matrices such as AMPS-modified PVA or PEG-sulfonate hydrogels retain drugs for multi-day release, whereas less-charged or more porous structures (*e.g.*, HepaSphere™) promote faster elution. Deformable hydrogels (PVA, PEG) navigate microcatheters efficiently and achieve distal embolization, while rigid or highly expandable systems can alter penetration depth within the vasculature.[102]

In 2025, a prospective, open-label, randomized phase IV trial[103] involving 239 patients with Barcelona Clinic Liver Cancer (BCLC) stage B hepatocellular carcinoma compared

idarubicin- and epirubicin-loaded DEBs. The idarubicin group demonstrated a significantly longer median progression-free survival (10.8 *vs.* 8.7 months; hazard ratio = 0.61; P = 0.002). In addition, overall survival rates at 12 and 24 months were higher in the idarubicin cohort (81.5% and 71.8%, respectively) compared to the epirubicin group (77.3% and 54.0%). The objective response rate was also significantly improved with idarubicin (70.8% *vs.* 57.1%, P = 0.03), indicating superior therapeutic efficacy.

3.1.2. MSs under development. Biodegradable polymer MSs are a major research focus for delivering cytotoxic drugs, aiming to avoid the long-term presence of permanent MSs. One example is poly (lactic-*co*-glycolic acid) (PLGA) MSs loaded with chemotherapeutics such as DOX. PLGA MSs can be formulated by emulsification[104] into a calibrated size (*e.g.* 26.36 ± 6.39 μm)[105] and provide drug release *via* erosion of the polymer matrix.[105] Unlike PVA hydrogels, which release drugs primarily by diffusion, PLGA hydrolytic degradation enables continuous drug release over days to weeks. The MSs ultimately resorb, resulting in temporary vessel occlusion. This transient embolization may reduce long-term vascular damage and allow reperfusion once the drug has acted.[105] *In vitro* study showed an initial burst with 35% cumulative DOX release in the first 2 days, followed by a plateau (63%) after 14 days.[106] Release kinetics can be tuned by adjusting PLGA formulations, such as lactic/glycolic ratio or polymer molecular weight.[107]

In addition, natural polymer-derived MSs have also been explored. Chitosan-based hydrogel MSs, often crosslinked with co-polymers like carboxymethyl cellulose, can be loaded with DOX and gradually dissolve *in vivo*.[108,109] The polycationic nature and gel porosity of chitosan enable high drug loading (0.085 mg DOX per mg MSs), swelling, and tunable resorption (hours to days). It provides controlled drug release and the potential for repeated embolization without leaving permanent emboli.[109] One patented formulation uses a carboxymethyl chitosan–carboxymethyl cellulose crosslinked matrix that is initially embolic but enzymatically degradable, allowing vessel recanalization in rabbit renal models within a few weeks.[110] These materials exhibit bio-adhesive properties that promote arterial retention and undergo hydrolytic degradation, enabling eventual clearance.[111]

3.2. Anti-angiogenic agents

Tumor embolization creates a hypoxic microenvironment that stimulates pro-angiogenic signalling pathways. Among these, upregulation of vascular endothelial growth factor (VEGF) can compromise therapeutic efficacy by promoting neovascularization and restoring blood supply to the treated tumor.[112] To address this response, anti-angiogenic agents have been integrated into MSs. By releasing anti-angiogenic agents locally within the embolized tissue, MSs can potentially suppress hypoxia-driven neovascularization and mitigate the pro-angiogenic rebound triggered by TACE.[80]

3.2.1. Anti-angiogenic agents combined with commercially available MSs. Although anti-angiogenic (AA) drugs have been widely studied in DEMs, none have yet achieved clinical adoption or commercialization. Existing PVA-based DEBs can be loaded with tyrosine kinase inhibitors (TKIs), small-molecule anti-angiogenic drugs such as sunitnib and sorafenib. For example, DC Bead™ was evaluated for loading sunitinib, which was absorbed into the hydrogel and released in a controlled manner *in vitro* and *in vivo*.[113] Embolization with sunitinib-eluting MSs produced a sustained increase up to around 35 ng mL^{-1} in plasma sunitinib levels, whereas oral administration of a single dose resulted in a decline from around 10 ng mL^{-1} to 7 ng mL^{-1} after 6 hours.[113]

Hagan *et al.*[114] loaded vandetanib into DC Bead™ (Fig. 10A) and DC Bead LUMI™ (Fig. 10B) for comparison. The release of vandetanib from both DC Bead™ and DC Bead LUMI™ into PBS exhibited an initial burst during the first 2 hours, followed by a gradual plateau phase (Fig. 10C). Over the full testing period, DC Bead™ demonstrated a higher cumulative release, reaching approximately 85% within 24 hours, whereas DC Bead LUMI™ released only about 50% on average. Notably, vandetanib elution from DC Bead LUMI™ did not reach completion, even though the maximum concentration in the release medium remained below the drug's theoretical solubility limit of 0.008 mg mL^{-1}.

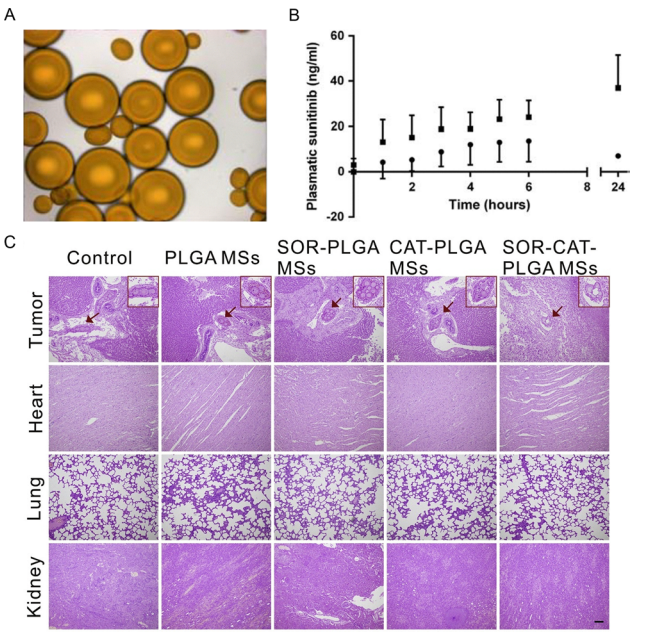

Fig. 10 (A). Image of vandetanib-loaded DC Bead™ (30 mg mL^{-1}, pH 4.6).[114] (B) Image of vandetanib-loaded DC Bead LUMI™ (100 mg mL^{-1}, pH 4.6).[114] (C) Vandetanib release profiles from DC Bead™ (●) and DC Bead LUMI™ (■), expressed as a percentage of the available drug dose. MSs (0.3 mL), containing the equivalent of 12 mg vandetanib, were incubated in 1 L of PBS (pH 7) under stirring. Data represent mean ± SD (n = 3).[114] (A), (B), and (C) are reproduced with permission from ref. 114. Copyright 2017, Elsevier. D. H&E-stained sections of excised liver tumors and major organs (lung, heart, kidney) from the control, PLGA MSs, Sorafenib-PLGA MSs, Catalase-PLGA MSs, and Sorafenib-Catalase-PLGA MSs groups.[115] MSs were detected within tumor-associated vasculature and surrounded by necrotic tissue, while no MSs were observed in healthy liver parenchyma. Red arrows indicate MSs. Scale bar = 100 μm. D is reproduced with permission from ref. 115. Copyright 2020, Elsevier.

In contrast, the release kinetics of sorafenib are different from those of ionic chemotherapeutics. Owing to its hydrophobic and weakly ionic, sorafenib interacts weakly to the PEG/PVA hydrogels,[116] leading to rapid elution with an initial burst within hours to a day.[117] Strategies such as co-loading with catalase have been proposed to slow the release and improve local retention.[115]

3.2.2. MSs under development. Experimental MS systems have been developed to enable local delivery of anti-angiogenic agents.[118,119] Although none have yet entered routine clinical practice, ongoing research demonstrates promising therapeutic potential. One notable example is resorbable embolization MSs (REM), designed to combine anti-angiogenic delivery with temporary embolization. Bédouet *et al.*[120] developed a one-day degradable MS containing 10–20% methacrylic acid. The methacrylic acid introduced carboxylate groups that enable efficient loading of sunitinib at levels comparable to DOX-DEBs. These REMs degrade within ~24 hours in aqueous media, releasing 30% of sunitinib in 1 hour, and releasing the remaining sunitinib linearly while gradually dissolving. *In vitro*, sunitinib-eluting REMs steadily released drug over several hours, and the eluate significantly inhibited endothelial cell and VX2 tumor cell proliferation, demonstrating preserved anti-angiogenic activity. Importantly, these MSs are completely resorbed, providing a temporary embolization that is sufficient to induce ischemia during peak drug release, while potentially allowing reperfusion. After cTACE, this strategy may enable localized anti-angiogenic therapy while minimizing systemic exposure. This has been approved by *in vivo* results. VX2 rabbit liver tumor models[115] were used to evaluate the antitumor efficacy of different MS formulations delivered through TACE. Histological analysis (Fig. 10D) demonstrated that Sorafenib-Catalase-PLGA MSs effectively occupied the tumor vasculature and induced almost complete tumor necrosis. Importantly, H&E staining of major organs-including the heart, liver, kidneys, and lungs-showed no apparent pathological changes, tissue damage, or inflammation.

Permanent and temporary embolic MS materials function differently in anti-angiogenic drug delivery. Permanent PVA/PEG MSs can load TKIs with incomplete drug release[113] with a durable embolization, but they are less suitable when vessel recanalization is desired for repeated chemoembolization procedures,[120] nor when monoclonal antibodies[121] is required. In contrast, degradable hydrogels such as PLGA-based systems allow more complete release of drug as the matrix itself breaks down. A key design challenge with degradable MSs is to balance degradation rate, since rapid resorption can lead to early reperfusion and reduced drug retention. To address this, modified systems have been explored, such as embedding forming sorafenib microcrystals inside MSs or by layering polyelectrolyte coatings onto MSs to trap the drug. Studies have shown that a layer-by-layer alginate-chitosan coating can achieve a near-linear release over days instead of a burst.[122]

A recent study[123] developed chondroitin sulfate-based MSs capable of co-delivering the chemotherapeutic agent idarubicin and Lenvatinib, aiming to address post-TACE tumor recurrence driven by hypoxia-induced angiogenesis. By incorporating Lenvatinib directly into the MSs, the system enables localized inhibition of VEGF signaling, overcoming the poor tumor penetration and systemic toxicity associated with oral anti-angiogenic therapy.

3.3. Hypoxia-activated prodrugs

Hypoxic is a hallmark of aggressive solid tumors and a major contributor to resistance to conventional therapies.[124] Hypoxia-activated prodrugs (HAPs) are an emerging class of anticancer agents developed to address the hypoxic tumor microenvironment. These prodrugs remain inactive under normoxic conditions but undergo enzymatic reduction in hypoxic regions to release potent cytotoxic payloads, thereby targeting resistant tumor subvolumes selectively while sparing normal tissue.[125] Thus, HAPs-loaded MSs have been widely studied, as TACE-induced hypoxia can serve as a natural ''trigger'' to active prodrugs and target hypoxic tumor cells.[126]

3.3.1. Commercially available MSs. Up to date, no HAP has been incorporated into commercial MSs, and no off-the-shelf embolic specifically designed for HAPs exists. In clinical practice, HAPs such as tirapazamine or evofosfamide have been administered systemically or intra-arterially alongside cTACE, for example, by mixing the prodrug with lipiodol or injecting it during embolization.[127,128] Due to the activation of the HAPs, it is critical to validate the stability of HAPs within the MS matrix and to confirm their activation within tumor tissue before clinical translation can be achieved.

CalliSpheres (PVA) MSs have been used in a study to carry tirapazamine, demonstrating that commercial DEBs can be loaded with HAPs.[129] In that study, the investigators pre-soaked CalliSpheres in a tirapazamine solution (Fig. 11 A) and delivered them by TACE in a VX2 rabbit liver tumor model. The results (Fig. 11B and C) showed that Tirapazamine-loaded Callispheres MSs therapy enhances tumor necrosis from 72.6% (TAE alone) to 99.5% (TPZ-loaded CalliSpheres). While this is not a regulated product, it shows that existing MS technology is compatible with HAP delivery (the MSs acted as a depot releasing tirapazamine into hypoxic tumor regions). However, because no regulatory-approved HAP-eluting MS is on the market, any such use remains experimental or off-label.

3.3.2. MSs under development. Among the HAPs investigated, evofosfamide (TH-302) has drawn particular attention. It is a 2-nitroimidazole prodrug of a DNA-alkylating agent that is selectively activated in hypoxic environments.[130] It has demonstrated enhanced efficacy in preclinical models and progressed into clinical evaluation.[131] Ma *et al.*[132] developed TH-302-loaded PLGA MSs for TACE, aiming to achieve localized delivery of prodrug to the tumor and use embolization-induced hypoxia to activate the prodrug intracellularly. The PLGA MSs were fabricated *via* an oil-in-water emulsion solvent evaporation method, producing spherical particles in three calibrated size ranges (75–100, 100–200, 200–300 μm), with TH-302 dispersed in the polymer matrix. *In vitro*, these MSs showed sustained TH-302 release (Fig. 11D) for up to 360 h (~15 days) as the PLGA gradually degraded. Under hypoxic conditions, the released drug exhibited enhanced cytotoxicity to cancer cells

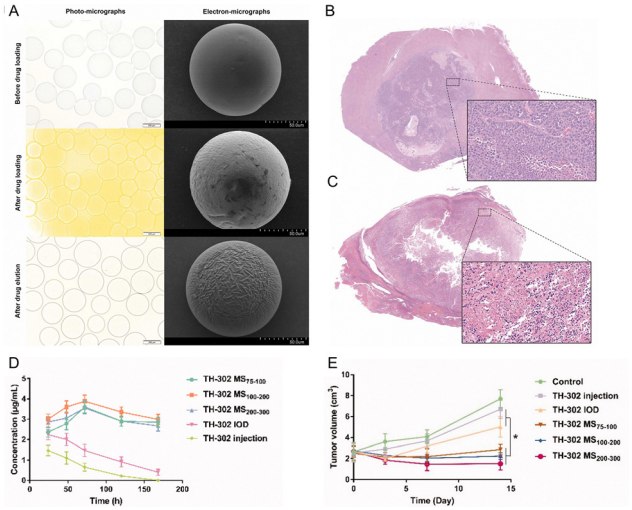

Fig. 11 (A) Micrographs of tirapazamine-loaded CalliSpheres® MSs before and after drug loading and after drug eluting;[129] (B) and (C). Tirapazamine-loaded CalliSpheres® MS therapy improves tumor necrosis.[129] Representative hematoxylin–eosin–stained sections (×10; inset ×400) of tumors treated with free tirapazamine B and with TPZ-loaded CSMs C. (A), (B), and (C) are reproduced with permission from ref. 129. Copyright 2022, Elsevier. (D) Liver tissue concentrations of TH-302 in rabbits (n = 3) following TACE using TH-302–loaded MSs, TH-302 mixed with iodized oil (IOD), or direct TH-302 injection.[132] E. Antitumor efficacy of TH-302 MS, TH-302 IOD, and TH-302 injection in VX2 tumor–bearing rabbits, shown as tumor volume change over 14 days after TACE.[132] D and E are reproduced with permission from ref. 132. Copyright 2020, Taylor & Francis.

(HepG2) than under normoxia, confirming that the prodrug was effectively activated under low-oxygen condition. In a rabbit liver tumor model (VX2), TACE with TH-302-PLGA MSs led to significantly greater tumor necrosis (Fig. 11E) and slower tumor growth than either cTACE or systemic TH-302. Importantly, no major systemic toxicity was observed, indicating that localized delivery spared normal tissues. This work demonstrates the feasibility of a biodegradable TH-302-eluting MS where the polymer ensures prolonged intratumoral prodrug presence and then safely resorbs.[133]

Metal-phenolic network-engineered MSs loaded with the hypoxia-activated prodrug TH302 have been developed[134] to exploit embolization-induced hypoxia. These systems enable hypoxia-triggered drug activation and pH-responsive release, resulting in enhanced tumor necrosis and improved therapeutic efficacy, highlighting the potential of hypoxia-responsive DEB in TACE.

3.4. Monoclonal antibodies

Monoclonal antibodies (mAbs) have emerged as key agents in solid tumor therapy due to their high specificity for tumor-associated antigens and multifaceted mechanisms of action.[130] Building on their success, recent research has investigated the integration of mAbs into drug-eluting embolic MSs for locoregional therapy, aiming to achieve high sustained intratumoral antibody concentrations while minimizing systemic exposure.[135]

3.4.1. Commercially available MSs. Monoclonal antibodies (*e.g.* bevacizumab, trastuzumab, or immunotherapy agents, such as nivolumab) are large (~150 kDa) proteins[136] that pose unique challenges for loading into MSs.[137] Developing MS systems capable of encapsulating large, hydrophilic protein therapeutics (such as full-length antibodies) remains challenging because of the intrinsic characteristics of these molecules, including their susceptibility to physical and chemical degradation, complex charge profiles, and tendency to self-associate or aggregate. These challenges are further compounded by fabrication methods that involve organic solvents and high shear forces.[138] Post-fabrication modifications to amino acid residues, such as isomerization, deamidation, and oxidation, along with protein aggregation or self-association, can significantly diminish the bioactivity of the therapeutic protein, leading to markedly reduced efficacy *in vivo*.[137] As a result, no vendor has released an antibody-eluting MS for clinical use.

Researchers have begun exploring ways to "arm" embolic MSs with monoclonal antibodies for localized therapy. One pioneering study by Sakr *et al.*[135] employed a layer-by-layer (LbL) assembly approach to load bevacizumab onto embolic MSs. In this method, the negatively charged DC Bead™ surface (due to sulfonate groups) was coated with positively charged polycations and layers of the antibody, building a multilayer film that entrapped bevacizumab on the MS (Fig. 12A). By changing the order of coating, lyophilization, and bevacizumab loading, drug loading in 2 hours can be tuned from 4% to 96%, and the drug release can be increased to 64% after 6 hours. This LbL-coated "immunobead" maintained bevacizumab's bioactivity (inhibiting endothelial cell proliferation *in vitro* (Fig. 12B) and demonstrated the feasibility of delivering large antibodies *via* catheter without clogging.

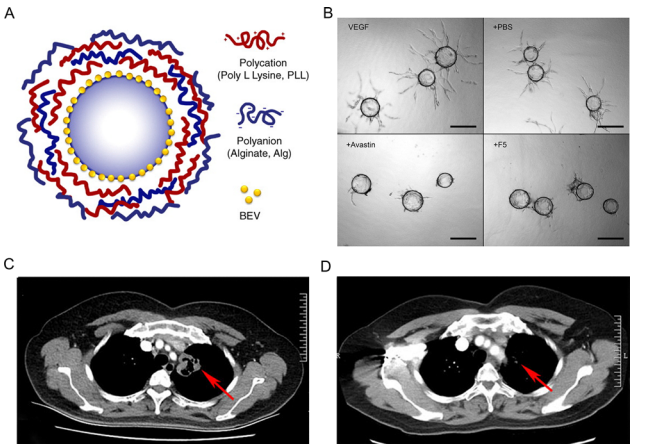

Fig. 12 (A) Schematic representation of BEV-loaded DC Bead® coated with alternating layers of alginate and poly-L-lysine.[135] (B) Endothelial cell viability following treatment with VEGF alone, VEGF + PBS, VEGF + Avastin, or VEGF + F5 MSs.[135] The results demonstrate the anti-angiogenic activity of BEV released from F5 MSs in a 3D fibrin MS sprouting assay. Bright-field images show Cytodex MSs with endothelial sprouts after 4 days in culture. Scale bar = 150 μm. (A) and (B) are reproduced with permission from ref. 135. Copyright 2016, Elsevier. (C and D) Clinical case of lung adenocarcinoma treated with BEV-loaded Callispheres®.[139] (C) Contrast-enhanced chest CT revealing cavitary lesions in the left upper lobe (arrow). (D) Post-treatment CT showing reduction in tumor size (arrow). (C) and (D) are reproduced with permission from ref. 139. Copyright 2023, Frontiers.

A case study conducted by Liu *et al.*[139] used Callispheres™ loaded with BEV for bronchial arterial chemoembolization. The treatment (Fig. 12C and D) achieved an objective response rate of 44% and a disease control rate of 100% following DEB-BACE. The 6- and 12-month overall survival rates were 77.8% and 66.7%, respectively, which indicates that bronchial arterial chemoembolization using BEV-loaded Callispheres™ MSs is both effective and well tolerated in patients with lung adenocarcinoma.

3.4.2. MSs under development. One research thrust involves degradable hydrogel MSs specifically designed to carry proteins. The one-day REM system mentioned earlier successfully loaded bevacizumab by incorporating methacrylic acid groups, achieving ~80–90% of the loading capacity seen with smaller drugs.[120] These MSs released intact bevacizumab over a few hours and then dissolved, showing that even without a multilayer shell, a suitably engineered hydrogel can carry an antibody locally. The key is to have enough charged sites to adsorb the antibody and a gentle release mechanism (MS degradation) to avoid protein deactivating. The REM MSs, being larger (100–300 μm), provided ample surface area and internal network for the antibody to distribute, and cytotoxicity tests confirmed that the blank MSs were cell-friendly.

Beyond VEGF-targeted therapy, there is interest in immune checkpoint inhibitors (ICIs) (such as anti-PD-1 or anti-CTLA4 antibodies) delivered directly into tumors *via* MSs to boost immune response. Early-stage research has looked at small-molecule checkpoint inhibitors (which are not antibodies but mimic their effect) loaded into MSs. For example, Negussie *et al.*[91] loaded a PD-1/PD-L1 inhibitor (BMS-202, a small molecule) and a toll-like receptor agonist (imiquimod) into radiopaque DC Bead LUMI™ particles. While not antibodies, this work demonstrates the concept of ''immunoembolization'' MSs that combine embolization with immune modulation. The drugs were successfully loaded by ion-exchange and released in a controlled fashion, around 70 μmol per mL of MSs in 72 hours, laying groundwork for eventually loading true biologic drugs. For actual mAbs, similar principles (surface attachment, hydrogel entrapment) would apply.

A recent study[140] demonstrated the feasibility of incorporating monoclonal antibody-based immunotherapy into embolic MSs by developing biodegradable MSs loaded with the anti-PD-L1 antibody envafolimab. Delivered *via* TACE, these MSs enabled sustained and localized immune checkpoint blockade within the tumor microenvironment. This approach effectively counteracted TACE-induced immunosuppression, particularly by reducing PD-L1$^+$ myeloid-derived suppressor cells and enhancing T-cell–mediated antitumor immunity. As a result, significantly improved tumor suppression was achieved compared to conventional treatments. This work provides direct evidence that monoclonal antibodies can be successfully integrated into DEB, highlighting their potential for localized immunotherapy in embolization-based cancer treatments.

In summary, monoclonal antibodies can be incorporated into MSs through tailored surface and network design strategies. Techniques like LbL deposition provide a controlled release reservoir for antibodies on MS surfaces,[135] and modified degradable hydrogels allow absorption and release of large biologics. No material has yet been proven fully optimal: PVA-based MSs needed surface coatings to effectively load bevacizumab,[135] while new hydrogel formulas (*e.g.* PVA/MA REM) can load mAbs but only retain for short durations (useful for burst release during embolization).[120] The material properties (pore size, charge density, degradability) directly impact loading efficiency (~milligrams of antibody per mL MSs) and release kinetics (hours *vs.* days). Each strategy could be tuned depending on the clinical need – a short intense local immunotherapy *vs.* a prolonged low-dose exposure. Though still experimental, these advances hint at future ''immunoembolization'' MSs that could deliver immune checkpoint inhibitors or other antibodies directly to the tumor microenvironment, potentially enhancing anti-tumor immunity with fewer systemic side effects.[91]

In conclusion, MS-based embolization spans a growing array of drug classes and therapeutic strategies. Comparative insights across materials and drug types are crucial: a PVA-sulfonate MS excellently delivers ionic chemotherapeutics but may require creative re-engineering (co-monomers, coatings) to handle proteins or hydrophobic molecules. Biodegradable polymers like PLGA bring flexibility for loading novel agents (TKIs, prodrugs, *etc.*) and ensure no permanent implant remains, while the release profile is more complex due to polymer breakdown.[132] Natural polymers (gelatin, starch, chitosan) offer transient occlusion and innate biocompatibility, which is advantageous for short-acting therapies like HAPs or gene vectors, yet their lower mechanical strength can limit precise calibration and delivery control.[141] Material selection for a given drug class is therefore a deliberate choice to optimize loading efficiency (ionic *vs.* hydrophobic interactions), release kinetics (diffusion *vs.* degradation-controlled), and embolic duration (temporary *vs.* permanent) for the therapeutic goal at hand. For future research, a critical priority is the tuning of mechanical properties of DEBs to improve occlusion[142,143] for creating better hypoxic environments. Current hydrogel-based MSs (*e.g.*, PVA, PEG) are compressible, but finer control of Young's modulus would allow MSs to navigate tortuous vessels while achieving secure occlusion.[144] Another potential avenue is the development of stimuli-responsive materials-responsive to pH, enzymes, temperature, or force-represent an exciting frontier for on-demand drug release within the unique tumor.

4. Discussion

4.1. Drug transport and release across embolic platforms

Embolic platforms exhibit fundamental differences in how they interact with the vascular environment. Low-viscosity embolic systems such as ethanol can access distal vasculature easily,[38] although this often comes at the expense of spatial control over embolic distribution. In contrast, lipiodol, with a viscosity relatively higher than blood, generates mechanical resistance within microvasculature, limiting its ability to navigate fine tumor vessels.[145] Moreover, if deep and stable distal deposition

is not achieved, lipiodol may be washed out, and is therefore sometimes combined with particles or coils to achieve more controlled and durable occlusion.[25]

In contrast, MS-based systems consist of discrete, size-controlled particulates suspended in carrier fluid. Their injectability is governed by both particle properties and suspension characteristics.[146] Upon delivery, MSs embolize tumor-feeding vessels in a size-dependent manner, producing localized intravascular occlusion, with penetration depth constrained by particle diameter. They form a stable occlusive structure through mechanical lodging and packing within the vasculature.[147]

Therapeutic agents are incorporated into embolic materials through multiple distinct mechanisms (Fig. 13). In liquid systems, drugs are primarily incorporated through solubilization or emulsification within a carrier phase.[14,19] In contrast, gel and MS embolic agents involve multiple concurrent mechanisms, including physical entrapment (*e.g.*, encapsulation or network entrapment), ionic or electrostatic interactions, adsorption, and covalent conjugation. These combined mechanisms, particularly physical entrapment mechanisms such as network entrapment and encapsulation, enable higher and more tunable drug incorporation potential[91] compared to liquid systems. This is because structured matrices and discrete carriers provide defined physical domains for drug confinement, in contrast to liquid systems where loading is constrained by phase behavior and solubility.[91]

Drug release behavior is governed by how drugs are incorporated within the material matrix. In liquid embolic platforms, drug release is driven by diffusion and phase separation, with release time within 24 hours.[29] Also, drug loading is clinically defined on a dose basis, representing the total amount administered per procedure. As a result, intrinsic loading capacity is less critical in liquid systems. In gel-based systems, release is controlled by network characteristics such as crosslinking density. This enables sustained release over days to weeks depending on material design, with reported drug loadings on the order of 25–50 mg mL^{-1} and sustained release ranging from several days to over 30 days depending on material design.[62] MS-based systems further shift toward controlled release through interaction-driven and encapsulation-based mechanisms, with commonly reported examples including ionic interactions and physical encapsulation. These systems are able to achieve higher loading capacities (approximately 45–200 mg mL^{-1})[91] and more predictable release profiles over days to weeks.[89] While in biodegradable MS, drug release is governed by polymer degradation, enabling prolonged drug release. Release kinetics can be further tuned through formulation design,[107] typically exhibiting an initial burst release during the first few days, followed by a sustained release phase (*e.g.*, plateau after ~14 days).[106]

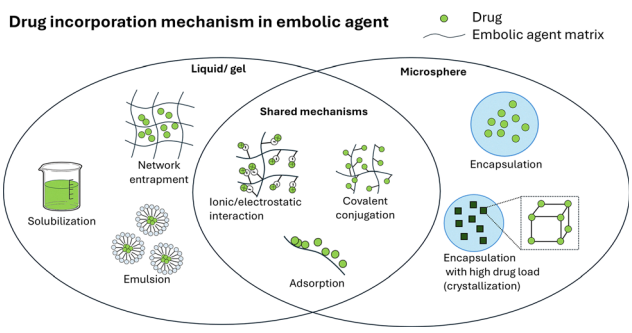

Fig. 13 Drug incorporation mechanism summary in embolic agents.

Overall, embolic agents exhibit distinct transport and drug delivery behaviors that arise from differences in material form and structure (Table 3). Liquid systems with low viscosity enable distributed drug delivery and deeper vascular penetration, while higher-viscosity systems such as lipiodol-based emulsions may exhibit limited or heterogeneous tumor penetration. MS-based systems are associated with localized intravascular occlusion and more controlled, sustained drug release, with penetration constrained by particle size. Gel-based systems occupy an intermediate position, enabling transient distal transport prior to gelation while providing tunable localization and release characteristics. These differences establish a continuum of embolic behavior across platforms, reflecting how material structure governs transport, localization, and release.

4.2. Design principle

Differences in embolic platforms translate into a set of interdependent design trade-offs that govern safe and effective embolization. Accordingly, therapeutic embolic agents should be designed as a multiparameter system, where material form and formulation define transport behavior, occlusion stability, and therapeutic function. The following sections outline the key trade-offs that establish the operational constraints for embolic performance.

4.2.1. Injectability *vs.* post-delivery stability. Injectability is primarily governed by viscosity and shear-dependent flow behavior, defining a fundamental trade-off between ease of delivery and post-injection structural integrity.[16] Lower viscosity or pronounced shear-thinning behavior reduces injection pressure and facilitates navigation through microcatheters and distal vasculature. However, excessive fluidity increases the risk of uncontrolled dispersion and non-target embolization. In MS-based systems, injectability is additionally governed by suspension stability, where particle sedimentation and aggregation must be minimized to ensure consistent delivery.[148] If not properly controlled, these factors may lead to catheter clogging, inconsistent delivery, or unintended embolization, resulting in non-target tissue ischemia and severe complications such as stroke.[10]

Following delivery, embolic agents must maintain effective occlusion under physiological pressure, requiring sufficient yield stress, viscoelasticity, and structural recovery. Materials with insufficient post-delivery stability may deform or migrate, whereas excessively stiff systems compromise injectability and increase catheter pressure.

In systems undergoing *in situ* transitions (*e.g.*, thermal- or pH-triggered gelation),[56] transition kinetics further constrain this trade-off. Slow transitions improve deliverability but increase distal migration, whereas rapid solidification enhances localization at the expense of injectability and catheter compatibility.

Table 3 Comparison of material characteristics and delivery performance across embolic platforms

	Liquid/gel systems	Microsphere systems
Material form	Continuous (fluid/hydrogel)	Discrete particles
Injectability	Flowable, viscosity-dependent	Particle suspension-dependent
Penetration	Deep, distal access/limited by viscosity	Limited by particle size
Drug release	Liquid: rapid; Gel: sustained	Sustained

Consequently, transition kinetics must be tuned relative to injection duration and local hemodynamics, defining a narrow operational design window.[10]

4.2.2. Penetration depth *vs.* localization precision. As discussed in Section 4.1, embolic platforms differ in their transport characteristics, reflecting a fundamental trade-off between penetration depth and localization precision. Increasing penetration depth enables access to distal vasculature but reduces spatial confinement, whereas improved localization limits dispersion at the expense of distal reach.

This trade-off arises from material form and transport behavior, where flowability, particle size, and phase transition determine spatial distribution within the vascular network. Accordingly, embolic systems should be designed to achieve an appropriate balance between distal access and controlled localization. Reduced localization precision increases the likelihood of off-target embolization, linking transport behavior to clinical risk.[16,17,147]

4.2.3. Degradability *vs.* functional persistence. The time-dependent behavior of embolic materials defines a trade-off between functional persistence and controlled degradation. Materials used for permanent embolization maintain structural integrity and sustain occlusion, whereas temporary embolic agents are designed to degrade in a controlled manner to restore blood flow.

Material properties such as degradation rate, swelling behavior, and solubility determine this balance. Faster degradation is associated with earlier loss of occlusion, while prolonged persistence is associated with potential chronic foreign body response or delayed tissue recovery.[149] As such, degradation behavior defines the functional lifetime of the embolic material relative to the therapeutic objective.

Beyond transport and mechanical considerations, embolic materials must satisfy biological and procedural requirements. Biocompatibility, hemocompatibility, and thrombogenicity influence host response, while imageability supports real-time procedural guidance. These factors may introduce competing effects, such as incorporation of imaging agents or biofunctional components can alter rheological behavior or influence material performance.

As a result, embolic design reflects a balance between procedural visibility, biological response, and mechanical function, where modifications to improve one aspect may influence others.

4.2.4. Drug incorporation design. As discussed in Section 4.1, embolic agents differ in both spatial distribution and temporal release behavior. Accordingly, a central trade-off exists between the extent of drug distribution within the vasculature and the rate of drug release, where broader distribution (liquid systems) is generally associated with faster, diffusion-driven release, while localized embolization (*e.g.*, MSs) exhibits more sustained, structure-dependent release.

Besides, material structure governs drug loading capacity, with systems that provide greater structural confinement (*e.g.*, MSs) and interaction sites generally enable higher loading compared to liquid embolic systems. However, optimal drug loading should be guided by clinical considerations, as increased loading does not necessarily translate into improved therapeutic outcomes.

5. Challenges and opportunities

5.1. Current research and clinical translation of therapeutic embolic agents

Fig. 14 summarizes the key milestones in the development of therapeutic embolic platforms and highlights the translational trajectory of the field. Since cTACE was first reported in 1982,[20] embolic agents have expanded from early liquid systems toward MS and hydrogel-based platforms, with ongoing efforts to improve localization, drug delivery, and treatment consistency. Importantly, liquid embolic approaches remain widely used in clinical practice due to their established efficacy, adaptability, and extensive clinical validation.

The transition from cTACE to DEB reflects a shift in design philosophy toward improving drug localization and reducing systemic exposure since the 1990s.[25] This concept evolved into drug-eluting bead systems, with early clinical investigations initiated around 2005[150] and the introduction of commercially available radiopaque DEBs in 2017.[151] Despite enabling more sustained and localized drug delivery, DEB-TACE has not consistently demonstrated superior clinical outcomes or reduced adverse effects compared to cTACE, leading to variable adoption in clinical practice.[21,152] Notably, lipiodol-based cTACE is an established clinical procedure and is commonly used as a control in comparative studies.

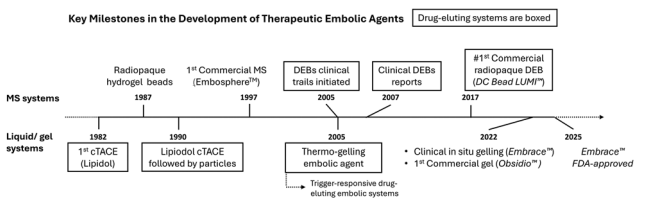

Fig. 14 Key milestones in the development of therapeutic embolic agents. Drug-eluting systems are highlighted with boxes.

Clinical comparisons between cTACE and DEB-TACE reveal distinct safety profiles, suggesting that DEB-TACE should be applied with caution. These findings also highlight the need for further optimization of both material design and drug incorporation strategies to achieve improved therapeutic outcomes with reduced adverse effects.

A randomized controlled study includes 200 patients in 2022[153] reported selective cTACE achieved higher CR rates for local tumor control as compared to selective DEB-TACE in HCC. In addition, a multicenter study includes 1002 patients in 2021[154] reported DEB-TACE was associated with a greater frequency of hepatobiliary injury and severe abdominal pain compared to cTACE. An earlier study in 2012[22] also suggest caution when using DEB-TACE, particularly in the non-cirrhotic liver. The study reported that liver and biliary injuries were independently associated with DEB-TACE, particularly in non-cirrhotic livers. Among these, biloma and liver infarction, the most severe complications, were significantly associated with DEB-TACE whereas such associations were not observed in cTACE-treated HCC.

A similar trajectory is emerging for gel-based embolic systems. Recent advances include non-drug-eluting, clinically available shear-thinning embolic systems (Obsidio[23]) and *in situ* forming gel embolic systems (Embrace[24]). In parallel, there is an increasing exploration of drug-loaded hydrogel formulations. These systems aim to complement existing platforms by improving spatial localization and enabling more controlled therapeutic delivery. However, their clinical translation remains at an early stage, with limited evidence compared to established liquid and MS-based systems.

5.2. Research opportunities and future therapeutic directions

Several emerging research directions have the potential to address current limitations and expand the therapeutic capabilities of embolization. Continued advances in material design are expected to enable embolic systems that combine mechanical robustness with controlled biodegradability, supporting stable occlusion while minimizing long-term vascular complications. These developments provide a foundation for incorporating a broader range of therapeutic payloads and release strategies.

Additionally, in response to the growing emphasis on non-animal testing methodologies, alternative preclinical evaluation strategies such as computational modeling are increasingly important. The development of digital twin models with personalized computational fluid dynamics for pre-therapy planning, optimizing the embolization procedure, and assessing the risk of off-target embolization is another direction. While MS-based computer models of embolization have been relatively more studied,[13,155–158] liquid and gel-based embolization have received less attention.[159,160]

Beyond conventional chemotherapeutics, embolic platforms are increasingly compatible with emerging therapeutic modalities. For example, immunomodulatory agents, including immune checkpoint inhibitors and cytokines, have already demonstrated feasibility in both liquid/gel-based and MS embolics. Looking ahead, embolization may also support delivery of larger[161–165] and more complex payloads such as nucleic-acid-based therapeutics (*e.g.*, siRNA, mRNA), viral vectors for gene therapy, and potentially cell-based therapies. The ability of embolic materials to localize and retain therapeutic agents within defined vascular territories offers a unique advantage for these modalities, particularly in minimizing systemic exposure and enhancing local efficacy.

Furthermore, combination therapies represent another underexplored opportunity. While multiple anticancer drugs have been successfully incorporated into embolic agents,[34] systematic investigation of multi-drug regimens, such as drug incorporation mechanisms and resulting material behaviors, remains limited[2] to predict performance; instead, drug incorporation mechanisms and resulting material behaviors. Sequential or staged release of complementary agents, such as cytotoxic drugs combined with anti-angiogenic or immunomodulatory therapies, could enable more effective control of tumor progression and recurrence. Material architectures that support differential release kinetics or spatial segregation of therapeutic agents offer a promising route to realizing such strategies.

Stimuli-responsive embolic systems further expand the therapeutic design space. In addition to enzyme-responsive or pH-sensitive materials, external triggering modalities such as ultrasound, laser irradiation, or near-infrared light provide opportunities for spatiotemporal control of drug release. Ultrasound-triggered embolics, for example, could leverage acoustic energy to modulate permeability or disrupt carrier networks on demand, while light-activated systems may enable precise activation in superficial or image-guided settings. These approaches align naturally with interventional workflows and imaging guidance already used during embolization procedures.

Together, these directions highlight the potential of embolization as more than a passive delivery vehicle. With continued integration of materials science, pharmacology, and interventional techniques, embolic platforms may evolve into adaptable therapeutic systems capable of delivering diverse payloads and responding dynamically to local or externally applied cues. Systematic preclinical evaluation will be essential to establish safety, efficacy, and reproducibility as these concepts move toward clinical translation.

5.3. Translation and standardization challenges

Beyond methodological advancement, research in therapeutic embolic agents should be driven by the broader objective of meaningful clinical translation, with the aim of improving patient care and saving lives.

The successful development of therapeutic embolization systems relies on the integration of mechanical reliability, controlled drug delivery, imaging visibility, and biocompatibility. Despite substantial progress at the laboratory and preclinical levels, translation to clinical practice and large-scale production remains constrained by the absence of standardized evaluation and manufacturing frameworks.

A major barrier to clinical translation is the lack of unified standards for assessing mechanical integrity and embolic

performance. Appropriate mechanical strength, toughness, flexibility, and durability are crucial to prevent embolic agent migration, non-target embolization, or vessel rupture that can result in severe adverse events such as ischemia or stroke. Although current studies often assess parameters such as compressibility, elasticity, and injectability, no unified testing framework or regulatory guideline exists to ensure cross-comparability between materials and platforms. Developing consistent mechanical and performance standards will be vital to ensure reproducible embolic behavior and reduce procedure-related risks.

Long-term safety evaluation remains insufficient for many emerging embolic systems. Although short-term cytotoxicity and hemocompatibility are commonly assessed, extended *in vivo* studies aligned with international standards such as ISO 10993 and FDA guidance are limited. In particular, large-animal investigations exceeding 90 days to evaluate chronic vascular response, recanalization, degradation behavior, and systemic exposure are limited. These gaps hinder risk assessment and delay clinical translation.

From a manufacturing perspective, most reported systems lack validation under Good Manufacturing Practice (GMP) conditions, including batch-to-batch consistency, formulation stability, and sterility assurance. Addressing these production and regulatory requirements will enable scalable manufacturing, regulatory approval, and eventual clinical adoption.

Additionally, the relatively short development history has limited the availability of clinical evidence. This is particularly evident for MSs, with some studies reporting inconsistent outcomes and adverse effects. As a result, further clinical validation and standardization are still needed. Overall, this progression helps explain why different embolic platforms coexist today and why key challenges in controlled therapeutic release and treatment predictability remain active areas of research.

Author contributions

Keren Zhao: conceptualization, project administration, literature search, writing – review & editing, overall manuscript organization. Peng Chen: literature search, writing – review & editing. George Varghese P. J.: literature search, writing – review & editing. Mohammad-Reza Hosseini-Siyanaki: literature search, writing – review & editing. Reza Talaie: literature search, writing – review & editing. Amirhossein Arzani: literature search, writing – review & editing. Charles Kim: literature search, writing – review & editing. Jingjie Hu: supervision, literature search, riting – review & editing.

Conflicts of interest

There are no conflicts to declare.

Data availability

No new data reported in this manuscript. All data is available in the parent articles.

Acknowledgements

The authors are grateful to North Carolina State University, the Ralph E. Powe Junior Faculty Enhancement Award, North Carolina Biotechnology Center, and the National Institutes of Health (NIBIB 1R03EB033633 and NIA 1R21AG083692) for financial support.

References

1 A. S. Mikhail, A. H. Negussie, M. Mauda-Havakuk, J. W. Owen, W. F. Pritchard, A. L. Lewis and B. J. Wood, Drug-eluting embolic microspheres: State-of-the-art and emerging clinical applications, 2021, preprint, DOI: 10.1080/17425247.2021.1835858.
2 T. de Baere, Y. Arai, R. Lencioni, J.-F. Geschwind, W. Rilling, R. Salem, O. Matsui and M. C. Soulen, *Cardiovasc. Intervent. Radiol.*, 2016, **39**, 334–343.
3 A. A. De Salles, T. D. Solberg, P. Mischel, T. F. Massoud, A. Plasencia, S. Goetsch, E. De Souza and F. Viñuela, *AJNR Am. J. Neuroradiol.*, 1996, **17**, 1451–1458.
4 J. J. Leyon, T. Littlehales, B. Rangarajan, E. T. Hoey and A. Ganeshan, *Curr. Probl. Diagn. Radiol.*, 2014, **43**, 35–53.
5 C. Gong, M.-S. Sun, R. Leng, H.-L. Ren, K. Zheng, S.-X. Wang, R.-M. Zhu and C.-M. Li, *Sci. Rep.*, 2023, **13**, 6936.
6 D. F. Vollherbst, C. M. Sommer, C. Ulfert, J. Pfaff, M. Bendszus and M. A. Möhlenbruch, *AJNR Am. J. Neuroradiol.*, 2017, **38**, 1377–1382.
7 J. Lopera, *Semin. Intervent. Radiol.*, 2010, **27**, 014–028.
8 J. Spies, *Semin. Intervent. Radiol.*, 2013, **30**, 340–346.
9 S. Bhatia, A. Bhatia, A. J. Richardson, K. Richardson, C. Issa, J. G. Kumar, H. Jalaiean, B. Kava and H. N. Shah, *J. Vasc. Int. Radiol.*, 2025, **36**, 456–466.
10 J. Hu, H. Albadawi, B. W. Chong, A. R. Deipolyi, R. A. Sheth, A. Khademhosseini and R. Oklu, *Adv. Mater.*, 2019, **31**, 1901071.
11 M. Pinkiewicz, M. Pinkiewicz, J. Walecki and M. Zawadzki, *J. Clin. Med.*, 2022, **11**, 7208.
12 M. T. Lawton, W. C. Rutledge, H. Kim, C. Stapf, K. J. Whitehead, D. Y. Li, T. Krings, K. terBrugge, D. Kondziolka, M. K. Morgan, K. Moon and R. F. Spetzler, *Nat. Rev. Dis. Primers*, 2015, **1**, 15008.
13 Y. Tatari, T. A. Smith, J. Hu and A. Arzani, *J. Biomech.*, 2024, **176**, 112320.
14 Y. Jiang, Y. Zhang, Z. Lu, X. Wang, S. Bai, Y. Chen, J. Mao and G. Liu, *Liquid embolic agents for interventional embolization*, Elsevier B. V., 2022, DOI: 10.1016/j.chphma.2021.09.008.
15 S. Vaidya, K. Tozer and J. Chen, *Semin. Intervent. Radiol.*, 2008, **25**, 204–215.
16 K. Zhao, G. P. J. Varghese, P. Chen and J. Hu, *J. Mech. Behav. Biomed. Mater.*, 2024, **152**, 106448.
17 K. Zhao, P. Chen, Z. Wang, G. P. J. Varghese, J. Liu and J. Hu, *Biomater. Adv.*, 2025, **174**, 214298.
18 O. Jordan, A. Denys, T. De Baere, N. Boulens and E. Doelker, *J. Vasc. Int. Radiol.*, 2010, **21**, 1084–1090.
19 J.-M. Idée and B. Guiu, *Crit. Rev. Oncol. Hematol.*, 2013, **88**, 530–549.
20 T. Konno, H. Maeda, I. Yokoyama, K. Iwai, K. Ogata, S. Tashiro, K. Uemura, M. Mochinaga, E. Watanabe, K. Nakakuma, T. Morinaga and Y. Miyauchi, *Gan to Kagaku Ryoho*, 1982, **9**, 2005–2015.
21 K. T. Brown, R. K. Do, M. Gonen, A. M. Covey, G. I. Getrajdman, C. T. Sofocleous, W. R. Jarnagin, M. I. D'Angelica, P. J. Allen, J. P. Erinjeri, L. A. Brody, G. P. O'Neill, K. N. Johnson, A. R. Garcia, C. Beattie, B. Zhao, S. B. Solomon, L. H. Schwartz, R. DeMatteo and G. K. Abou-Alfa, *J. Clin. Oncol.*, 2016, **34**, 2046–2053.
22 B. Guiu, F. Deschamps, S. Aho, F. Munck, C. Dromain, V. Boige, D. Malka, S. Leboulleux, M. Ducreux, M. Schlumberger, E. Baudin and T. de Baere, *J. Hepatol.*, 2012, **56**, 609–617.
23 Boston Scientific, Obsidio, https://www.bostonscientific.com/en-US/medical-specialties/interventional-radiology/interventional-oncology/obsidio-conformable-embolic/about-obsidio.html?gclid=Cj0KCQjwm6POBhCrARIsAIG58CIBdBuIZcQL9LPrRe61_4J9aG2aq_lC4WWe8ki-wcd-xHV-Hz5x2fAaAhW2EALw_wcB&gad_source=1&gad_campaignid=21182142607&gbraid=0AAAApmNzAINJrz-mq0RlCafV8u8t3tkY, (accessed 28 March 2026).

24 *U.S. FOOD & DRUG, Embrace(TM) Hydrogel Embolic System Premarket Approval*, https://www.accessdata.fda.gov/scripts/cdrh/cfdocs/cfpma/pma.cfm?id=P250003, (accessed 28 March 2026).
25 H. Uchida, H. Ohishi, N. Matsuo, K. Nishimine, S. Ohue, Y. Nishimura, M. Maeda and T. Yoshioka, *Cardiovasc. Intervent. Radiol.*, 1990, **13**, 140–145.
26 B. Bonnemain and M. Guerbet, *Rev. Hist. Pharm.*, 1995, **42**, 159–170.
27 T. Kanematsu, K. Inokuchi, K. Sugimachi, T. Furuta, T. Sonoda, S. Tamura and K. Hasuo, *J. Surg. Oncol.*, 1984, **25**, 218–226.
28 Y. Idezuki, M. Sugiura, S. Hatano and S. Kimoto, *Surgery*, 1966, **60**, 566–572.
29 H. Nakamura, T. Hashimoto, H. Oi and S. Sawada, *Radiology*, 1989, **170**, 783–786.
30 K. Bannangkoon, K. Hongsakul and T. Tubtawee, *Sci. Rep.*, 2024, **14**, 18979.
31 H. Maeda and T. Konno, *Neocarzinostatin*, Springer Japan, Tokyo, 1997, pp. 227–267.
32 T. de Baere, X. Zhang, B. Aubert, G. Harry, C. Lagrange, J. Ropers, J. Dufaux, J. Lumbroso, P. Rougier, M. Ducreux and A. Roche, *Radiology*, 1996, **201**, 731–735.
33 Q. Shi, D. Chen, C. Zhou, J. Liu, S. Huang, C. Yang and B. Xiong, *Cancer Manage. Res.*, 2020, **12**, 5461–5468.
34 L. Marelli, R. Stigliano, C. Triantos, M. Senzolo, E. Cholongitas, N. Davies, J. Tibballs, T. Meyer, D. W. Patch and A. K. Burroughs, *Cardiovasc. Intervent. Radiol.*, 2007, **30**, 6–25.
35 C.-M. Lo, H. Ngan, W.-K. Tso, C.-L. Liu, C.-M. Lam, R. T.-P. Poon, S.-T. Fan and J. Wong, *Hepatology*, 2002, **35**, 1164–1171.
36 B. A. Ellman, B. J. Parkhill, T. S. Curry, P. B. Marcus and P. C. Peters, *Radiology*, 1981, **141**, 619–626.
37 T. Saguchi, Y. Arai, S. Kamei, A. Komemushi and K. Saito, *Interventional Radiol.*, 2018, **3**, 44–65.
38 B. Le Dare, T. Gicquel and B. Le Daré, Therapeutic Applications of Ethanol: A Review, *J. Pharm. Pharm. Sci.*, 2019, **22**, 525–535.
39 W. J. Earthman, M. J. Mazer and A. C. Winfield, *Radiology*, 1986, **160**, 437–441.
40 B. B. Lee, Y. S. Do, H. S. Byun, I. W. Choo, D. I. Kim and S. H. Huh, *J. Vasc. Surg.*, 2003, **37**, 533–538.
41 Y. Sawada, M. Shimohira, T. Hashizume, R. Sobue, S. Mori, M. Nakagawa, Y. Ozawa, T. Naiki, T. Nagai, T. Yasui and Y. Shibamoto, *Cardiovasc. Intervent. Radiol.*, 2017, **40**, 1933–1939.
42 C. M. Chick, B. Tan, C. Cheng, M. Taneja, R. Lo, Y. Tan, S. Lin and K. Tay, *BJU Int.*, 2010, **105**, 390–394.
43 N. Miyazono, K. Ueno, M. Nakajo, H. Nishida, H. Inoue, S. Tsuchimochi, H. Hokotate and H. Yoshida, *Invest. Radiol.*, 1996, **31**, 755–760.
44 W. F. Yakes, J. M. Luethke, J. J. Merland, K. M. Rak, D. D. Slater, H. W. Hollis, S. H. Parker, A. Casasco, A. Aymard, J. Hodes, K. D. Hopper, A. Thomas Stavros and T. E. Carter, *J. Vasc. Int. Radiol.*, 1990, **1**, 89–96.
45 U. Rimon, M. Duvdevani, A. Garniek, G. Golan, P. Bensaid, J. Ramon and B. Morag, *Am. J. Roentgenol.*, 2006, **187**, 762–768.
46 M. Sasaki, S. Tadokoro, S. Kimura, M. Mori, S. Kosuda and M. Tachibana, *Hinyokika Kiyo*, 1984, **30**, 295–298.
47 W. F. Yakes, J. M. Luethke, S. H. Parker, A. T. Stavros, K. M. Rak, K. D. Hopper, J. N. Dreisbach, D. J. Griffin, C. E. Seibert and T. E. Carter, *RadioGraphics*, 1990, **10**, 787–796.
48 X. D. Fan, L. X. Su, J. W. Zheng, L. Z. Zheng and Z. Y. Zhang, *AJNR Am. J. Neuroradiol.*, 2009, **30**, 1178–1183.
49 T. Kanematsu, K. Inokuchi, K. Sugimachi, T. Furuta, T. Sonoda, S. Tamura and K. Hasuo, *J. Surg. Oncol.*, 1984, **25**, 218–226.
50 Y. Matsumaru, A. Hyodo, T. Nose, S. Ito, T. Hirano and S. Ohashi, *J. Biomater. Sci., Polym. Ed.*, 1996, **7**, 795–804.
51 L. Klouda and A. G. Mikos, *Eur. J. Pharm. Biopharm.*, 2008, **68**, 34–45.
52 A. M. Pragatheeswaran, S. B. Chen, C.-F. Chen and B.-H. Chen, *Polymer*, 2014, **55**, 5284–5291.
53 Y. He, T. Yuan, X. Wang, M. Shen, L. Ding, L. Huang, S. Wang, P. Kong, X. Zhou, Y. Duan and J. Cao, *Mater. Sci. Eng. C*, 2020, **111**, 110798.
54 K. Qian, Y. Ma, J. Wan, S. Geng, H. Li, Q. Fu, X. Peng, X. Kan, G. Zhou, W. Liu, B. Xiong, Y. Zhao, C. Zheng, X. Yang and H. Xu, *J. Controlled Release*, 2015, **212**, 41–49.
55 B. A. Ellman, B. J. Parkhill, T. S. Curry, P. B. Marcus and P. C. Peters, *Radiology*, 1981, **141**, 619–626.
56 W. T. Godbey, K. K. Wu and A. G. Mikos, *J. Controlled Release*, 1999, **60**, 149–160.
57 A. Poursaid, R. Price, A. Tiede, E. Olson, E. Huo, L. McGill, H. Ghandehari and J. Cappello, *Biomaterials*, 2015, **57**, 142–152.
58 M. Haider, J. Cappello, H. Ghandehari and K. W. Leong, *Pharm. Res.*, 2008, **25**, 692–699.
59 Z. Megeed, M. Haider, D. Li, B. W. O'Malley, J. Cappello and H. Ghandehari, *J. Controlled Release*, 2004, **94**, 433–445.
60 Z. Megeed, J. Cappello and H. Ghandehari, *Pharm. Res.*, 2002, **19**, 954–959.
61 J. Cappello, J. W. Crissman, M. Crissman, F. A. Ferrari, G. Textor, O. Wallis, J. R. Whitledge, X. Zhou, D. Burman, L. Aukerman and E. R. Stedronsky, *J. Controlled Release*, 1998, **53**, 105–117.
62 A. Poursaid, M. M. Jensen, I. Nourbakhsh, M. Weisenberger, J. W. Hellgeth, S. Sampath, J. Cappello and H. Ghandehari, *Mol. Pharm.*, 2016, **13**, 2736–2748.
63 A. Poursaid, M. M. Jensen, I. Nourbakhsh, M. Weisenberger, J. W. Hellgeth, S. Sampath, J. Cappello and H. Ghandehari, *Mol. Pharm.*, 2016, **13**, 2736–2748.
64 A. Fatimi, P. Chabrot, S. Berrahmoune, J.-M. Coutu, G. Soulez and S. Lerouge, *Acta Biomater.*, 2012, **8**, 2712–2721.
65 F. Zehtabi, P. Ispas-Szabo, D. Djerir, L. Sivakumaran, B. Annabi, G. Soulez, M. A. Mateescu and S. Lerouge, *Acta Biomater.*, 2017, **64**, 94–105.
66 A. Fatimi, P. Chabrot, S. Berrahmoune, J.-M. Coutu, G. Soulez and S. Lerouge, *Acta Biomater.*, 2012, **8**, 2712–2721.
67 J. Kim, H. Keum, H. Albadawi, I. Altinbasak, F. Yavuz, E. H. Graf, N. Mishra and R. Oklu, *Adv. Mater.*, 2025, **37**, 2503179.
68 E. Kizilay, A. B. Kayitmazer and P. L. Dubin, *Adv. Colloid Interface Sci.*, 2011, **167**, 24–37.
69 M. Liu, Y. Sun, Y. Zhou, Y. Chen, M. Yu, L. Li, L. Yan, Y. Yuan, J. Chen, K. Zhou, H. Shan and X. Peng, *Adv. Healthcare Mater.*, 2024, **13**, 2304488.
70 M. Liu, Y. Sun, Y. Zhou, Y. Chen, M. Yu, L. Li, L. Yan, Y. Yuan, J. Chen, K. Zhou, H. Shan and X. Peng, *Adv. Healthcare Mater.*, 2024, **13**, 2304488.
71 G. Varghese P. J., K. Zhao, P. Chen and J. Hu, *J. Biomed. Mater. Res. A*, 2024, **112**, 914–930.
72 K. Zhao, G. P. J. Varghese, P. Chen and J. Hu, *J. Mech. Behav. Biomed. Mater.*, 2024, **152**, 106448.
73 W. Norde, *Colloids and Interfaces in Life Sciences and Bionanotechnology*, CRC Press, 2nd edn, 2011.
74 P. Kensbock, D. E. Demco, S. Singh, K. Rahimi, R. Fechete, A. Walther, A. M. Schmidt and M. Möller, *Langmuir*, 2017, **33**, 66–74.
75 J. Hu, H. Albadawi, Z. Zhang, M. A. Salomao, S. Gunduz, S. Rehman, L. D'Amone, J. L. Mayer, F. Omenetto and R. Oklu, *Adv. Mater.*, 2022, **34**, 2106865.
76 N. Falcone, M. Ermis, A. Gangrade, A. Choroomi, P. Young, T. G. Mathes, M. Monirizad, F. Zehtabi, M. Mecwan, M. Rodriguez, Y. Zhu, Y. Byun, A. Khademhosseini, N. R. de Barros and H.-J. Kim, *Adv. Funct. Mater.*, 2024, **34**, 2309069.
77 N. S. Gunasekara, D. Faulds, P. Beale and A. L. Jackman, Raltitrexed A Review of its Pharmacological Properties and Clinical Efficacy in the Management of Advanced Colorectal, *Cancer*, 1998, DOI: 10.2165/00003495-199855030-00012.
78 Q. Qian, D. Wang, L. Shi, Z. Zhang, J. Qian, J. Shen, C. Yu and X. Zhu, *Biomaterials*, 2021, **265**, 120403.
79 Y. Peng, H. Liu, X. Liang, L. Cao, M. Teng, H. Chen, Z. Li, X. Peng, J. Mao, H. Cheng and G. Liu, *J. Controlled Release*, 2025, **380**, 1–16.
80 A. S. Mikhail, A. H. Negussie, M. Mauda-Havakuk, J. W. Owen, W. F. Pritchard, A. L. Lewis and B. J. Wood, *Expert Opin. Drug Delivery*, 2021, **18**, 383–398.
81 J. E. Song and D. Y. Kim, *World J. Hepatol.*, 2017, **9**, 808–814.
82 N. Damle and P. Frost, *Curr. Opin. Pharmacol.*, 2003, **3**, 386–390.
83 S. Carter and R. C. G. Martin, *HPB*, 2009, **11**, 541–550.
84 W. Yoon, *Expert Opin. Pharmacother.*, 2004, **5**, 361–367.
85 A. L. Lewis and R. R. Holden, *Expert Opin. Drug Delivery*, 2011, **8**, 153–169.
86 K. Ashrafi, Y. Tang, H. Britton, O. Domenge, D. Blino, A. J. Bushby, K. Shuturminska, M. den Hartog, A. Radaelli, A. H. Negussie, A. S. Mikhail, D. L. Woods, V. Krishnasamy, E. B. Levy, B. J. Wood, S. L. Willis, M. R. Dreher and A. L. Lewis, *J. Controlled Release*, 2017, **250**, 36–47.

87 H. C. Nam, B. Jang and M. J. Song, *World J. Gastroenterol.*, 2016, **22**, 8853.
88 A. L. Lewis, M. V. Gonzalez, S. W. Leppard, J. E. Brown, P. W. Stratford, G. J. Phillips and A. W. Lloyd, *J. Mater. Sci.: Mater. Med.*, 2007, **18**, 1691–1699.
89 A. L. Lewis, M. V. Gonzalez, A. W. Lloyd, B. Hall, Y. Tang, S. L. Willis, S. W. Leppard, L. C. Wolfenden, R. R. Palmer and P. W. Stratford, *J. Vasc. Int. Radiol.*, 2006, **17**, 335–342.
90 R. R. Taylor, Y. Tang, M. V. Gonzalez, P. W. Stratford and A. L. Lewis, *Eur. J. Pharm. Sci.*, 2007, **30**, 7–14.
91 A. H. Negussie, A. S. Mikhail, J. W. Owen, N. Hong, C. J. Carlson, Y. Tang, K. P. Carrow, M. Mauda-Havakuk, A. L. Lewis, J. W. Karanian, W. F. Pritchard and B. J. Wood, *Sci. Rep.*, 2022, **12**, 21886.
92 R. T. P. Poon, W. K. Tso, R. W. C. Pang, K. K. C. Ng, R. Woo, K. S. Tai and S. T. Fan, *Clin. Gastroenterol. Hepatol.*, 2007, **5**, 1100–1108.
93 T.-Y. Zhou, S.-Q. Chen, H.-L. Wang, S.-M. Weng, G.-H. Zhou, Y.-L. Zhang, C.-H. Nie, T.-Y. Zhu, B.-Q. Wang, Z.-N. Yu, L. Jing, F. Chen and J.-H. Sun, *J. Cancer*, 2021, **12**, 4522–4529.
94 K. Malagari, A. Pomoni, D. Filippiadis and D. Kelekis, *Hepat. Oncol.*, 2015, **2**, 147–157.
95 B. Liu, S. Gao, J. Guo, F. Kou, S. Liu, X. Zhang, A. Feng, X. Wang, G. Cao, H. Chen, P. Liu, H. Xu, Q. Gao, R. Yang, L. Xu and X. Zhu, *J. Hepatocell. Carcinoma*, 2024, **11**, 477–488.
96 O. Jordan, A. Denys, T. De Baere, N. Boulens and E. Doelker, *J. Vasc. Int. Radiol.*, 2010, **21**, 1084–1090.
97 T. de Baere, S. Plotkin, R. Yu, A. Sutter, Y. Wu and G. M. Cruise, *J. Vasc. Int. Radiol.*, 2016, **27**, 1425–1431.
98 T. Tanaka, H. Nishiofuku, Y. Hukuoka, T. Sato, T. Masada, M. Takano, C. W. Gilbert, C. Obayashi and K. Kichikawa, *J. Vasc. Int. Radiol.*, 2014, **25**, 1037–1044.e2.
99 N. A. Nuzulia, T. Mart, I. Ahmed and Y. W. Sari, *ACS Biomater. Sci. Eng.*, 2024, **10**, 637–656.
100 F. Pan, D. Schneider, E. Ryschich, B. Qian, D. F. Vollherbst, M. A. Möhlenbruch, M. Jugold, V. Eichwald, P. Stenzel, P. L. Pereira, G. M. Richter, H. U. Kauczor, C. M. Sommer and T. D. Do, *Cardiovasc. Intervent. Radiol.*, 2020, **43**, 636–647.
101 G. Jia, J. Van Valkenburgh, A. Z. Chen, Q. Chen, J. Li, C. Zuo and K. Chen, *Wiley Interdiscip. Rev.: Nanomed. Nanobiotechnol.*, 2022, **14**, e1749.
102 W. M. Hetta and N. Shebria, *The Egyptian Journal of Radiology and Nuclear Medicine*, 2014, **45**, 761–769.
103 H. Liu, W. Fan, H. Li, L. Qiao, Z. Liu, B. Zhu, J. Guo, K. Huang, Y. Tang, J. Wen, M. Xue, Y. Wu, Y. Zhao, Y. Jiang, K. Liu, J. Liang, M. Cao and J. Li, *Radiology*, 2025, **315**, 2.
104 Y. Su, B. Zhang, R. Sun, W. Liu, Q. Zhu, X. Zhang, R. Wang and C. Chen, *Drug Delivery*, 2021, **28**, 1397–1418.
105 J. W. Choi, J.-H. Park, S. Y. Baek, D.-D. Kim, H.-C. Kim and H.-J. Cho, *Colloids Surf., B*, 2015, **132**, 305–312.
106 B. Amoyav, A. I. Bloom, Y. Goldstein, R. Miller, M. Sharam, A. Fluksman and O. Benny, *Adv. Healthcare Mater.*, 2023, **12**, 2301548.
107 H. K. Makadia and S. J. Siegel, *Polymers*, 2011, **3**, 1377–1397.
108 L. Weng, H.-J. Tseng, P. Rostamzadeh and J. Golzarian, *J. Mater. Sci.: Mater. Med.*, 2016, **27**, 174.
109 L. Weng, P. Rostamzadeh, N. Nooryshokry, H. C. Le and J. Golzarian, *Acta Biomater.*, 2013, **9**, 6823–6833.
110 L. Weng, D. Seelig, P. Rostamzadeh and J. Golzarian, *J. Vasc. Int. Radiol.*, 2015, **26**, 1887–1894.e1.
111 H. Cai, A. Li, F. Qi, R. Liu, X. Tang, D. Li, Y. Gu and J. Liu, *Mater. Adv.*, 2024, **5**, 3094–3112.
112 H. Mahaki, S. Nobari, H. Tanzadehpanah, A. Babaeizad, G. Kazemzadeh, M. Mehrabzadeh, A. Valipour, N. Yazdinezhad, H. Manoochehri, P. Yang and M. Sheykhhasan, *Biomed. Pharmacother.*, 2025, **186**, 118023.
113 K. Fuchs, P. E. Bize, O. Dormond, A. Denys, E. Doelker, G. Borchard and O. Jordan, *J. Vasc. Int. Radiol.*, 2014, **25**, 379–387.e2.
114 A. Hagan, G. J. Phillips, W. M. Macfarlane, A. W. Lloyd, P. Czuczman and A. L. Lewis, *Eur. J. Pharm. Sci.*, 2017, **101**, 22–30.
115 X. Li, H. Yu, Y. Huang, Y. Chen, J. Wang, L. Xu, F. Zhang, Y. Zhuge and X. Zou, *Biomed. Pharmacother.*, 2020, **129**, 110512.
116 S. K. Shukla, M. Goyal, D. D. Kanabar, S. Ayehunie, B. Deore, C. A. Sanhueza, A. Muth and V. Gupta, *J. Mol. Liq.*, 2024, **401**, 124701.
117 G. Babos, E. Biró, M. Meiczinger and T. Feczkó, *Polymers*, 2018, **10**, 895.
118 G. M. Tozer, C. Kanthou and B. C. Baguley, *Nat. Rev. Cancer*, 2005, **5**, 423–435.
119 A. M. Al-Abd, A. J. Alamoudi, A. B. Abdel-Naim, T. A. Neamatallah and O. M. Ashour, *J. Adv. Res.*, 2017, **8**, 591–605.
120 L. Bédouet, V. Verret, S. Louguet, E. Servais, F. Pascale, A. Beilvert, M.-T. Baylatry, D. Labarre, L. Moine and A. Laurent, *Int. J. Pharm.*, 2015, **484**, 218–227.
121 A. L. Lewis and M. R. Dreher, *J. Controlled Release*, 2012, **161**, 338–350.
122 O. S. Sakr, S. Berndt, G. Carpentier, M. Cuendet, O. Jordan and G. Borchard, *J. Controlled Release*, 2016, **224**, 199–207.
123 J.-X. Huang, R. Yang, H. Long, J. Kong, G.-Q. Shao and F. Xiong, *Mater. Today Bio*, 2025, **30**, 101419.
124 F. W. Hunter, B. G. Wouters and W. R. Wilson, *Br. J. Cancer*, 2016, **114**, 1071–1077.
125 L. Spiegelberg, R. Houben, R. Niemans, D. de Ruysscher, A. Yaromina, J. Theys, C. P. Guise, J. B. Smaill, A. V. Patterson, P. Lambin and L. J. Dubois, *Clin. Transl. Radiat. Oncol.*, 2019, **15**, 62–69.
126 Q. Li, J. Shi, X. Ruan, L. Zhang, R. Fu, K. Hidayat, L. Qin, J. Xu, Y. Chong and C. Hu, *Adv. Funct. Mater.*, 2025, **35**, e10798.
127 N. Abi-Jaoudeh, F. Dayyani, P. J. Chen, D. Fernando, N. Fidelman, H. Javan, P.-C. Liang, J.-I. Hwang and D. K. Imagawa, *J. Hepatocell. Carcinoma*, 2021, **8**, 421–434.
128 C.-H. Liu, C.-M. Peng, J.-I. Hwang, P.-C. Liang, P.-J. Chen, N. Abi-Jaoudeh, L.-H. Giiang and Y.-S. Tyan, *J. Vasc. Int. Radiol.*, 2022, **33**, 926–933.e1.
129 Q. Li, Y. Liu, X. Guo, L. Zhang, L. Li, D. Zhao, X. Zhang, W. Hong, C. Zheng and B. Liang, *Biomed. Pharmacother.*, 2022, **151**, 113123.
130 J.-X. Duan, H. Jiao, J. Kaizerman, T. Stanton, J. W. Evans, L. Lan, G. Lorente, M. Banica, D. Jung, J. Wang, H. Ma, X. Li, Z. Yang, R. M. Hoffman, W. S. Ammons, C. P. Hart and M. Matteucci, *J. Med. Chem.*, 2008, **51**, 2412–2420.
131 R. M. Phillips, *Cancer Chemother. Pharmacol.*, 2016, **77**, 441–457.
132 P. Ma, J. Chen, H. Qu, Y. Li, X. Li, X. Tang, Z. Song, H. Xin, J. Zhang, J. Nai, Z. Li and Z. Wang, *Drug Delivery*, 2020, **27**, 1412–1424.
133 Z. Wang, Q. Li and B. Liang, *Pharmaceuticals*, 2024, **17**, 1057.
134 Q. Li, J. Shi, X. Ruan, L. Zhang, R. Fu, K. Hidayat, L. Qin, J. Xu, Y. Chong and C. Hu, *Adv. Funct. Mater.*, 2025, **35**, e10798.
135 O. S. Sakr, S. Berndt, G. Carpentier, M. Cuendet, O. Jordan and G. Borchard, *J. Controlled Release*, 2016, **224**, 199–207.
136 J. T. Ryman and B. Meibohm, *CPT: Pharmacometrics Syst. Pharmacol.*, 2017, **6**, 576–588.
137 S. Iyer, C. Lee and M. M. Amiji, *Drug Delivery Transl. Res.*, 2025, **15**, 3149–3160.
138 D. Blanco and M. J. Alonso, *Eur. J. Pharm. Biopharm.*, 1998, **45**, 285–294.
139 H. Liu, Y. Li, Z. Li, X. Han and K. Ren, *Front. Pharmacol.*, 2023, **14**, 1170344.
140 H. Liu, J. Huang, Z. Wang, N. Wang, X. Hao, Y. Chai, N. Yu, H. Cao, Y. He, S. Dai, J. Xu, Z. Zhang, J. Kong, F. Xiong, W. Tang and J. Song, *ACS Appl. Mater. Interfaces*, 2026, **18**, 4979–4994.
141 H. Cai, A. Li, F. Qi, R. Liu, X. Tang, D. Li, Y. Gu and J. Liu, *Mater. Adv.*, 2024, **5**, 3094–3112.
142 P. Chen, G. P. J. Varghese, K. Zhao and J. Hu, *J. Mech. Behav. Biomed. Mater.*, 2024, **160**, 106739.
143 P. Chen, S. Jernigan, K. Zhao, G. P. J. Varghese, M. Saha, C. Kim, A. Arzani, G. Buckner and J. Hu, *Biomater. Sci.*, 2025, **13**, 4786–4802.
144 X. Li, M. W. Ullah, B. Li and H. Chen, *Adv. Healthcare Mater.*, 2023, **12**, 2202787.
145 M. Caine, T. Chung, H. Kilpatrick, Z. Bascal, S. Willis, Y. Tang, T. de Baere, M. Dreher and A. Lewis, *Theranostics*, 2019, **9**, 5626–5641.
146 P. Chen, G. P. J. Varghese, K. Zhao and J. Hu, *J. Mech. Behav. Biomed. Mater.*, 2024, **160**, 106739.
147 K. Fuchs, R. Duran, A. Denys, P. E. Bize, G. Borchard and O. Jordan, *Drug-eluting embolic microspheres for local drug delivery - State of the art*, Elsevier B.V., 2017, preprint, DOI: 10.1016/j.jconrel.2017.07.016.
148 A. Lundbäck, F. Snidare, R. Silfur, A. Mokhbat and C. Gunasekara, Uppsala University, Department of Materials Science and Engineering, 2025.
149 J. M. Anderson, A. Rodriguez and D. T. Chang, *Semin. Immunol.*, 2008, **20**, 86–100.

150 *National Institutes of Health, Chemoembolization Using Doxorubicin in Treating Patients With Liver Cancer That Cannot Be Removed By Surgery*, https://clinicaltrials.gov/study/NCT00293397, (accessed 28 March 2026).
151 *Boston Scientific, DC Bead LUMI™*, https://www.bostonscientific.com/en-EU/products/embolics/dc-bead-lumi.html, (accessed 28 March 2026).
152 A. Facciorusso, M. Di Maso and N. Muscatiello, *Dig. Liver Dis.*, 2016, **48**, 571–577.
153 M. Ikeda, Y. Arai, Y. Inaba, T. Tanaka, S. Sugawara, Y. Kodama, T. Aramaki, H. Anai, S. Morita, Y. Tsukahara, H. Seki, M. Sato, K. Kamimura, K. Azama, M. Tsurusaki, E. Sugihara, M. Miyazaki, T. Kobayashi and M. Sone, *Liver Cancer*, 2022, **11**, 440–450.
154 L. Zhang, J.-H. Sun, J.-S. Ji, B.-Y. Zhong, G.-H. Zhou, J.-J. Song, Z.-H. Hou, P. Huang, S. Zhang, Z. Li, X.-L. Zhu and C.-F. Ni, *Am. J. Roentgenol.*, 2021, **217**, 933–943.
155 T. J. Snoeijink, T. G. Vlogman, J. Roosen, E. Groot Jebbink, K. Jain and J. F. W. Nijsen, *Drug Delivery*, 2022, 2226366.
156 J. Aramburu, R. Antón, M. Rodríguez-Fraile, B. Sangro and J. I. Bilbao, *Cardiovasc. Intervent. Radiol.*, 2022, **45**, 12–20.
157 E. Roncali, A. Taebi, C. Foster and C. T. Vu, *Ann. Biomed. Eng.*, 2020, **48**, 1499–1510.
158 M. Mahmoudi, C. Jennings, K. Pereira, A. F. Hall and A. Arzani, *J. Biomech. Eng.*, 2022, **144**, 111004.
159 W. Wang, F. Graziano, V. Russo, A. J. Ulm, D. De Kee and D. B. Khismatullin, *Biorheology*, 2013, **50**, 99–114.
160 G. Sema, S. Zamani, T. Touris, F. Norpetlian, L. Whitney, A. Zhao, C. Zhou, S. Konangi and M. Sami, *Med. Eng. Phys.*, 2025, **144**, 104394.
161 K. Yang, K. Ma, M. Yang, Y. Lv, Y. Pei and Z. Pei, *Chem. Commun.*, 2023, **59**, 3779–3782.
162 T. Kang, Q. Zhu, D. Wei, J. Feng, J. Yao, T. Jiang, Q. Song, X. Wei, H. Chen, X. Gao and J. Chen, *ACS Nano*, 2017, **11**, 1397–1411.
163 J. Liu, J. Liu, W. Mu, Q. Ma, X. Zhai, B. Jin, Y. Liu and N. Zhang, *ACS Nano*, 2024, **18**, 20861–20885.
164 S. Cao, Z. Pei, Y. Xu and Y. Pei, *Chem. Mater.*, 2016, **28**, 4501–4506.
165 X. Jiang, W. Han, J. Liu, J. Mao, M. J. Lee, M. Rodriguez, Y. Li, T. Luo, Z. Xu, K. Yang, M. Bissonnette, R. R. Weichselbaum and W. Lin, *Adv. Sci.*, 2022, **9**, 2201614.